Wave Theory Based Data Preparation for Inverse Scattering Multiple Removal, Depth Imaging and Parameter Estimation: Analysis and Numerical Tests of Green's Theorem Deghosting Theory

---

A Dissertation

Presented to

the Faculty of the Department of Physics

University of Houston

In Partial Fulfillment

of the Requirements for the Degree

Doctor of Philosophy

By

Jingfeng Zhang

December 2007

Wave Theory Based Data Preparation for Inverse Scattering Multiple Removal, Depth Imaging and Parameter Estimation: Analysis and Numerical Tests of Green's Theorem Deghosting Theory

---

Jingfeng Zhang

APPROVED:

Dr. Arthur B. Weglein, Chairman

Dr. Kristopher A. Innanen

Dr. Wei-Kan Chu

Dr. Kenneth Matson

Dr. Simon Shaw

Dr. David J. Francis

Dr. Wolfgang Donner

Dean, College of Natural Sciences and Mathematics

ACKNOWLEDGMENTS

In the Fall of 2001, I came to America for my PhD in Physics. In the last six years, I have received a lot of education, help and encouragement from Prof. Weglein. I am deeply grateful for all of them. Prof. Weglein is an interesting combination of high technical capability, some special personality and street smarts. He came from the New York street, got a B.S. in Mathematics in a highly competitive college, acquired a Ph.D. in Physics with a famous Professor, then went to the energy industry to work on Geophysics and had a successful 30 years of life, after that came to UH become a full professor and started a consortium which is supported by over 20 major oil and service companies around the world. Having this kind of life, no doubt he has a lot of stuff to teach, both technically and non-technically. Fortunately for his students, including myself, he is willing to teach all of the things (again, both technically and non-technically) that he thinks are helpful for the growth of his students. I have to say that I am very lucky to have him as my advisor.

I would like to thank Simon Shaw who was a great colleague in M-OSRP and is a great role model. Especially, I want to thank him and Rob Habiger for providing me my first ever industry experience. I also want to thank Douglas Foster for his kind support when I was at ConocoPhillips.

I want to thank Ken Matson for his help and encouragements for my dissertation and, of course, for the great internship at BP. He was there to discuss and help me on every important part of my project at BP. Without his help, it would be very difficult for me to have a successful internship and get an offer.

I appreciate the support of Jon Sheiman on this research. I would like to thank Kris Innanen, Fang Liu, Bogdan Nita, Adriana Ramírez, Einan Otnes, Gustavo Correa and Haiyan Zhang for all of the help they have given to me. Especially I want to thank Bogdan for his help on writing this dissertation.

I am grateful for all of the help and advice that Chris Weglein has offered to help Haiyan and myself to take care of my daughter Rachel. Taking care of Rachel has been a big part of my life and can affect my research work if not done right. As the parents of four fine sons, she and Prof. Weglein certainly know a lot in child care and education. Their advice is very valuable because Haiyan and myself are still learning to be good parents.

Special thanks to my parents, parents-in law, and my wife Haiyan for their help, dedication and encouragements.

Wave Theory Based Data Preparation for Inverse Scattering Multiple Removal, Depth Imaging and Parameter Estimation: Analysis and Numerical Tests of Green's Theorem Deghosting Theory

---

An Abstract of a Dissertation

Presented to

the Faculty of the Department of Physics

University of Houston

In Partial Fulfillment

of the Requirements for the Degree

Doctor of Philosophy

By

Jingfeng Zhang

December 2007

ABSTRACT

A new Green's theorem deghosting algorithm is developed, analyzed and tested. The deghosting algorithm requires both pressure and its vertical derivative on the measurement surface. For most conventional acquisition geometries, only pressure measurements are available. This dissertation provides a method to obtain stable deghosting results using conventional pressure data measurements. Numerical tests are tested for both point receiver and receiver array data.

The deghosted data are input to the inverse scattering series free surface multiple removal algorithm. The deghosted data predicted by the deghosting algorithm allows the free surface multiple removal algorithm to precisely predict and eliminate free surface multiples.

The deghosting algorithm is tested on ocean bottom data. Instead of directly using the noisy geophone measurements, the vertical derivative of pressure is calculated through the triangle relationship among source wavelet, pressure and its vertical derivative.

CONTENTS

1. INTRODUCTION AND BACKGROUND

In this chapter, I will provide some background information about seismic exploration. Seismic acquisition and data processing will be briefly introduced. The definition of and motivation for deghosting are also presented and discussed. The contribution, development and advances represented in this thesis will be delineated and defined within the context of a broader campaign to address pressing seismic challenges. An overview of this dissertation is also provided in this introduction.

1.1 General seismic exploration background

The objective of seismic exploration is to locate hydrocarbon reservoirs [1] in the earth. In marine seismic exploration (which I focus on in this dissertation), a boat moves in the water towing air-guns and streamers consisting of receivers [2](Fig. 1.1). The air-guns generate seismic waves that propagate into the earth. When a wave hits an interface, part of the wave will be reflected back to the receivers. The wavefield recorded by the receivers constitutes the seismic data that is going to be processed for exploration objectives.

The goal of exploration seismic processing is to locate and delineate those interfaces in

[1] A subsurface body of rock having sufficient porosity and permeability to store and transmit fluids. Sedimentary rocks are the most common reservoir rocks because they have more porosity than most igneous and metamorphic rocks and form under temperature conditions at which hydrocarbons can be preserved. A reservoir is a critical component of a complete petroleum system. -From Schlumberger Oilfield Glossary: www.glossary.oilfield.slb.com

[2] In common marine seismic exploration, the receiver is a hydrophone which is a device designed for use in detecting seismic energy in the form of pressure changes under water.

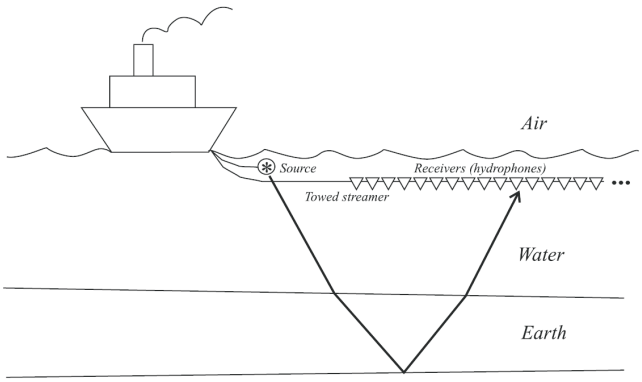

Fig. 1.1: *Marine seismic exploration geometry: * and ∇ indicate the source and receiver, respectively. The boat moves through the water towing the source and receiver arrays and the experiment is repeated at a multiple of surface locations. The collection of the different source-receiver wavefield measurements defines the seismic reflection data. (courtesy of Weglein* et al. *(2002))*

the earth (called imaging/migration) and then to identify the physical properties of targets (called inversion/Amplitude-Versus-Offset analysis/parameter identification) within a given region. Before achieving that goal of imaging and inversion, a series of tasks is often needed to pre-process the data. A typical data processing sequence in seismic exploration is:

- Data interpolation and extrapolation;
- Source wavelet estimation;
- Deghosting;
- Free surface multiple removal/attenuation;
- Internal multiple removal/attenuation;
- Velocity analysis (to be used in interface location) followed by
- Imaging and
- Inversion.

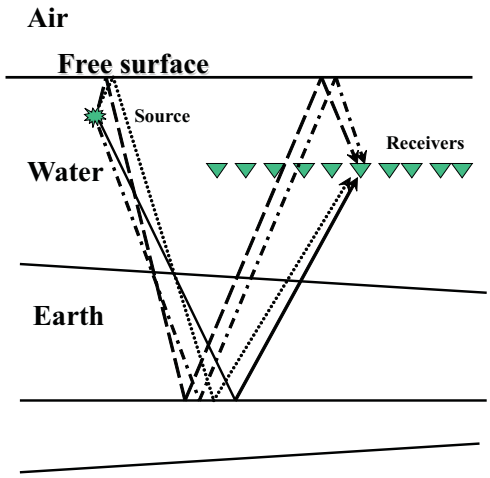

Fig. 1.2: *Primary and its ghosts. Solid line: Primary; Dotted line: Source ghost of primary; Dashed-dot line: Receiver ghost of primary; Dashed line: Source-receiver ghost of primary.*

The actual definitions of source wavelet, ghost/deghosting, free surface and internal multiple will be provided later in this chapter. The point of the list above is that seismic processing is a linked sequence or chain of steps, where the effectiveness of any given step not only depends upon how well its own assumptions are satisfied, but also how well all the earlier tasks in the chain have been achieved. Deghosting, as discussed in the next section, not only is required for conventional data processing, but also is a critical part of the new efforts to address outstanding and pressing seismic exploration and production challenges described in the next section.

In the following, I will provide a set of definitions of seismic terms relevant to the problem being addressed and the method to address that problem. Seismic data recorded by receivers are a collection of seismic events [3] which include primaries, multiples, the direct wave and their ghosts. Weglein *et al.* (2003) provide the definitions of these events. In this

[3] A seismic event is a temporally localized arrival of seismic energy.

dissertation, I choose a slightly different way to explain each event in order to emphasize the role of ghosts. Primaries are seismic events that travel *down* from the source to the earth, experience *one* upward reflection, and then travel *up* to the receivers (Fig. 1.2). *Each* primary is accompanied by three ghost events: its source ghost, receiver ghost and source-receiver ghost (Fig. 1.2). A primary and its ghosts have been reflected by the same interface in the earth. The difference is that instead of directly traveling *down* to the earth from the source, a source ghost travels *up* from the source to the air-water interface first, then it is reflected downward into the earth. For a receiver ghost, instead of directly traveling up to the receivers, it propagates up to the air-water interface first, then is reflected down to the receivers. The source-receiver ghost of a primary has a similar travel path as the primary in the earth; however, at the source side, it travels up from the source to the air-water interface first before it travels down to the earth, *and* on the receiver side, it travels up to the air-water interface first before it is reflected down from the air-interface to the receivers. Multiples are seismic events that travel *down* from the source to the earth, then experience more than one upward reflections in the earth, and then travel *up* to the receivers (Fig. 1.3). Just like primaries, each multiple is accompanied by three ghosts. Multiples are further separated into free surface and internal multiples, according to whether or not they have been reflected by the free surface (air-water interface). If a multiple has been reflected by the free surface, then it is a free surface multiple. Otherwise, it is an internal multiple. A free surface multiple is called an $n'th$ order free surface multiple if it is reflected by the free surface n times (Fig. 1.3). The process of removing all ghosts is called deghosting. Besides ghosts, the developed deghosting algorithm in this dissertation can also remove the reference wave, if it has not been removed before deghosting. The reference wave includes the direct wave which travels directly from the source to the receiver (Fig. 1.4) [4] and its ghost. After deghosting, at least three quarters of the seismic events will be removed.

[4] Receivers are typically towed at deeper depth than source.

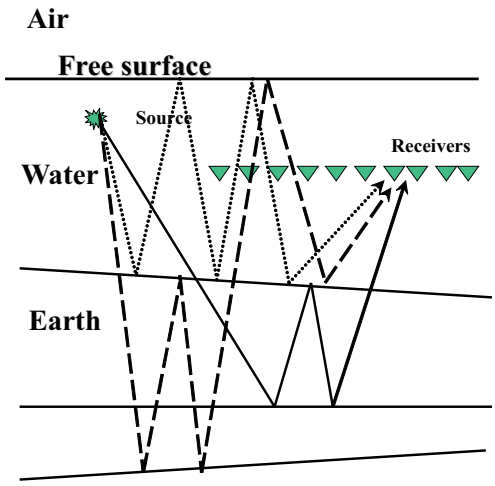

Fig. 1.3: *Free surface and internal multiples. Solid line: internal multiple; Dashed line: First order free surface multiple; Dotted line: Second order free surface multiple.*

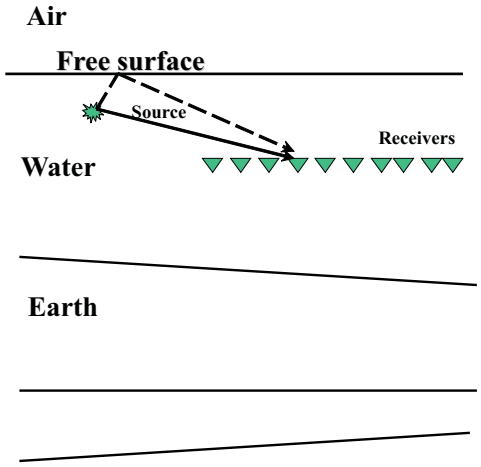

Fig. 1.4: *Direct wave and its ghost. Solid line: Direct wave; Dashed line: Ghost of direct wave.*

Since the direct wave and its ghost only travel in the water, they do not contain any information about the earth. This justifies their removal in processing methods that seek to delineate subsurface properties. But all other events contain information about the subsurface, so why do they need to be removed too? One reason for multiple removal is that there is no adequate algorithms to decipher the information they contain. Multiples are more complicated compared to primaries, which experience only one upward reflection in the earth. Why is it necessary to remove ghosts? One can argue that there is no adequate algorithm to use them either, just like multiples. But there are more compelling arguments about for it is necessary to remove ghost events. These are described in the next section.

1.2 Motivations for deghosting

In this section, I will list the arguments for deghosting seismic data.

1. Ghost events distort the data spectrum. Consider the receiver side as an example. The interference between the down-going wave and the up-going wave will be destructive to the spectrum of the up-going wave, since ghost notches (explained below) will be generated. I can demonstrate this point with a simple $1D$ normal incidence model. In Fig. 1.5, the free surface is placed at $z = 0$, and the receiver depth at $z = z_b$. Assume there is a wave propagating upward: $A(\omega)e^{-ikz}$ where $A(\omega)$ is its spectrum and k is the wavenumber ω/c , with c as the wave velocity. The amplitude spectrum of the up-going wave at receiver $z = z_b$ would be $|A(\omega)|$. After summing up with the down-going ghost event, the amplitude spectrum of the wavefield received at $z = z_b$ becomes $|A(\omega)e^{-ikz_b} - A(\omega)e^{ikz_b}| = 2|A(\omega)sin(kz_b)|$. This amplitude spectrum is the original $|A(\omega)|$ adjusted by $|sin(kz_b)|$. Whenever $kz_b = n\pi, (n = 0, 1, 2, 3, \cdots)$, the amplitude spectrum of the up- and down-going wave at those frequencies will be zero. Those frequencies are $f = nc/(2z_b), n = 0, 1, 2, 3, \cdots$. These zeroes in the amplitude

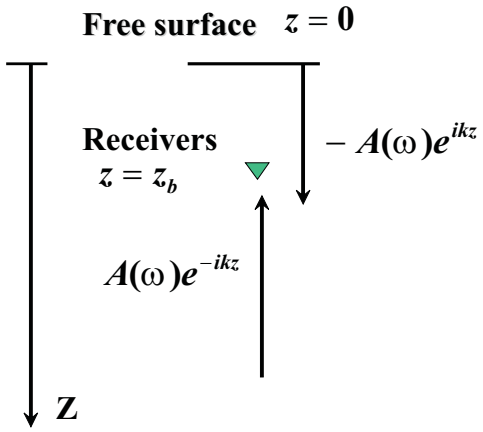

Fig. 1.5: *The* $1D$ *model used to demonstrate the spectral distortion due to ghost events. The free surface is at* $z = 0$ *and the receiver depth is at* $z = z_b$.

spectrum due to ghost events are called ghost notches. For the case of $c = 1500m/s$ and $z_b = 6.0m$, the first ghost notch is about $125Hz$ (Fig. 1.6).

There are two notes about Fig. 1.6. (1) In practice, $125Hz$ is usually much higher than the dominant frequency of the seismic data. So the effect of the ghost notch seems not very obvious for this kind of shallow receiver depth, except that missing high frequency information can affect the resolution of the earth image. However, (2) the low frequency (close to zero frequency) part of spectrum is always dampened by $|sin(kz_b)|$, which can be a serious issue because low frequencies are very important for algorithms like internal multiple removal [5] and the imaging of deep interfaces [6].

If the depth of the receiver increases, then the first ghost notch will appear at a lower frequency. For ocean bottom data, the first ghost notch can appear at very low

[5] The prediction of one frequency of internal multiple needs all frequencies of the data (Araújo, 1994; Weglein *et al.*, 1997; Ramírez and Weglein, 2005)

[6] Compared to low frequency signals, the energy of high frequency signals is more easily absorbed by the earth. So high frequency signals reflected by very deep earth are usually much weaker, which makes them difficult to use especially if they are weaker than random noise.

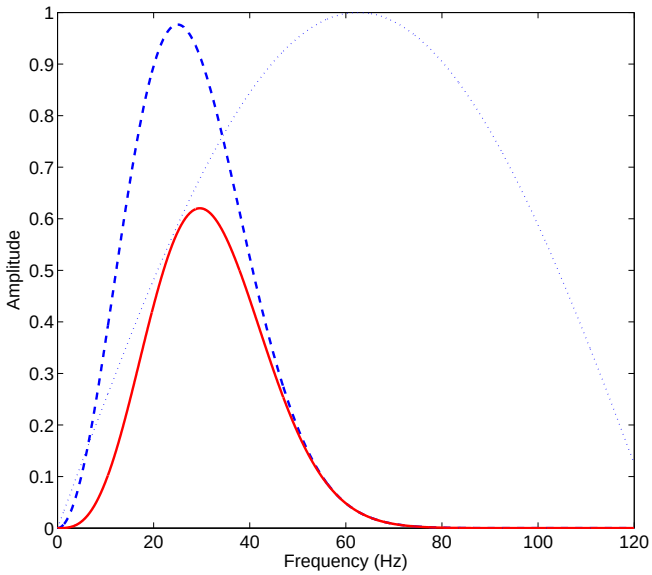

Fig. 1.6: *Illustration of the spectrum distortion of the data due to ghosts events/down-going wave. Dashed line: Amplitude spectrum of up-going wave; Dotted line: $sin(kz_b)$; Solid line: Amplitude spectrum of up and down-going waves arriving together at receiver. The receiver depth is 6.0m and the first ghost notch is around $125Hz$.*

frequency. For example, if $z_b = 200m$, then the first ghost notch is at $f = 3.75Hz$ (Fig. 1.7). The original amplitude spectrum of the up-going wave has been greatly distorted by the frequent appearance of the ghost notches. The information contained in the frequencies around those ghost notches is often not usable in practice since the signal can be below the ambient noise level.

2. Ghost effects can affect Amplitude-Versus-Offset (AVO) analysis. AVO is a procedure to determine the earth's properties by analyzing the amplitude variation of the data with respect to offset [7]. The effect of a ghost on the data varies with offset, so the existence of ghost events affects the AVO prediction. New inversion algorithms, like the direct nonlinear inversion derived from the inverse scattering series (Zhang and Weglein, 2005a, 2006) will be particularly affected by ghost events since they have high requirements on the accuracy of *primary* amplitudes. This means both the

[7] The horizontal distance between the source and receiver

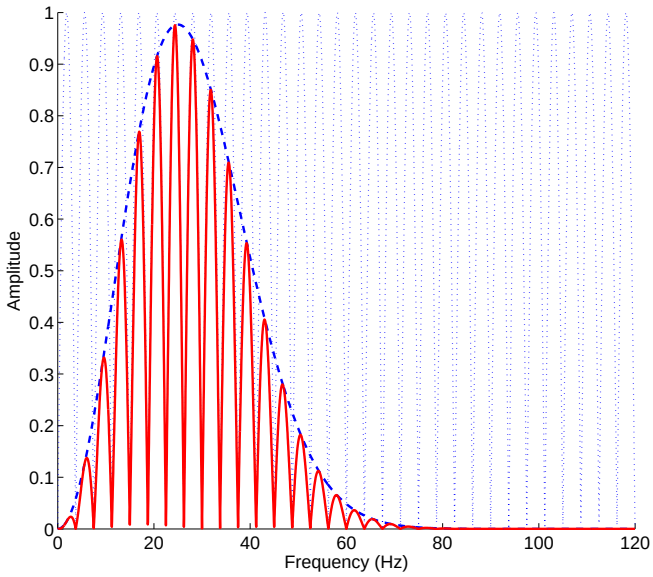

Fig. 1.7: *Illustration of the spectrum distortion of the data due to ghosts events/down-going wave. Dashed line: Amplitude spectrum of up-going wave; Dotted line:* $sin(kz_b)$*; Solid line: Amplitude spectrum of up and down-going waves arriving together at the receiver. The receiver depth is* $200m$ *and the first ghost notch is at* $3.75Hz$*.*

source signature and the ghosts must be removed.

3. Deghosting is a pre-requisite for the free surface multiple removal algorithm derived from the inverse scattering series (ISS) (Carvalho, 1992; Weglein *et al.*, 1997). There are many different free surface multiple removal algorithms (e.g., Carvalho (1992); Weglein *et al.* (1997); Verschuur *et al.* (1992); Matson and Abma (2005); Matson and Zhang (2007)), each with different assumptions, advantages and limitations. The ISS free surface multiple removal method and the feedback loop method (Verschuur *et al.*, 1992) do not need any subsurface information, which is a big advantage, especially under conditions of complex geology. Both methods need to predict free surface multiples before they can be removed from the data. The difference is that the ISS method has the ability to accurately predict the free surface multiples while the feedback loop method can only provide approximate predictions. That is the reason why the ISS method can remove the predicted multiples through a simple subtraction while

the feedback method has to remove the multiples "adaptively" using certain criterion (energy minimization, for example) (Verschuur *et al.*, 1992; Abma *et al.*, 2005). The energy minimization criterion assumes the energy of the data will be minimized after the multiples are removed. It is certainly true in areas where there is no overlap between primaries and multiples. If primaries and multiples overlap and destructively interfere, however, the energy after the removal of multiples will not necessarily be minimal. In this case, the energy minimization criterion fails and the adaptive subtraction will not work very well. ISS free surface multiple removal method can in principle predict the multiples accurately by (1) performing deghosting; (2) requiring the source wavelet; (3) including the obliquity factor and (4) taking into account the fact that the depths of the source and receiver are not at the water-air interface. Zhang and Weglein (2005b) have demonstrated that by providing all of the requirements above, the ISS free surface multiple removal algorithm accurately predicts free surface multiples which were later removed from the data by a simple subtraction. The results will be presented in this dissertation (see Chapter 3). In practice, due to issues such as the using of receiver array data [8], inaccurate source wavelet estimation and a non-planar, time-varying water-air interface, it is very difficult to accurately predict the free surface multiples. Hence, the adaptive subtraction is always important in practice. The point is to provide the algorithm's requirements as completely as possible, so that the burden of the adaptive subtraction can be reduced , especially in areas where adaptive subtraction has difficulties.

4. Dethosting is a pre-requisite for the internal multiple elimination method derived from ISS. The ISS internal multiple *attenuation* algorithm (Araújo, 1994; Weglein *et al.*,

[8] Receiver array is widely used in practice. A receiver array consists of certain number of receivers. The recordings of each receiver within an array is summed up to produce one output. Through the summation process, the signal/noise ratio can be improved based upon the assumption that phase of the random noise are all different while the phase of the signal are more or less the same. At the same time, the reference wave can be greatly reduced too.

1997) predicts internal multiples *approximately*, after which they need to be removed by adaptive subtraction. For this algorithm, deghosting may not make much difference. However, for the internal multiple *elimination* method (Ramírez and Weglein, 2005; Ramírez, 2007), deghosting is critical. The reason is that this elimination algorithm predicts the internal multiple accurately using primaries. The existence of primary ghosts will damage these predictions.

5. Deghosting is a pre-requisite for the imaging without the velocity method derived from the ISS (Weglein *et al.*, 2000, 2001; Shaw *et al.*, 2002; Innanen and Weglein, 2003; Liu *et al.*, 2005). Conventional imaging algorithms (F-K migration, finite difference migration) require the wave velocity in the subsurface. This velocity dependence makes these algorithms less sensitive to the amplitude of the data. The disadvantage is in areas where the velocity is difficult to obtain or the estimated velocity is not accurate enough, then these velocity dependent imaging algorithms will fail. With the current trend to explore and produce in deep water, besides the associated higher acquisition and drilling cost, higher risk, and technical challenges, there is also a pressing seismic challenge: image below complex and often ill-defined overburden medium where a satisfactory velocity is difficult to obtain. As a response to that challenge, the ISS imaging without the velocity method does not require the subsurface medium velocity, which makes it a good candidate in these complex areas. Compared to conventional imaging algorithms, this method places a higher bar on the data pre-processing. It requires that the data contain only primaries and that all other events (direct wave, multiples and all ghosts) are removed.

In the above, I have listed the reasons for deghosting. It is worthwhile to note that when there is a seismic processing challenge, there are two ways to address it: (1) try to develop methods that will help to satisfy the assumptions behind an algorithm and (2) develop a

fundamentally new algorithms that avoids the difficult to satisfy assumptions. Compared to the conventional imaging algorithms which require the velocity, the ISS imaging without the velocity method takes the second path. For deghosting, however, there is no candidate method available today that can achieve the aims and objectives (restoring the up-going wave spectrum) of ghost removal without removing the ghost. Hence, the only route for advancing our capability of achieving the goals behind ghost removal is to advance methods that can more effectively remove ghosts.

There is extensive literature about performing deghosting. Schneider *et al.* (1964) remove the ghost effects by using a numerical filter. Robertsson and Kragh (2002) and Amundsen *et al.* (1995) remove ghost events in frequency-wavenumber domain. The first method above works in time domain where it is difficult to find one single filter that works for all offsets of data. The latter two are wave theoretic methods and have some capabilities of dealing with rough sea deghosting. However, methods working in frequency-wavenumber domain often have the stableness issue. The deghosting method developed in this dissertation is a wave theoretic method and it works in frequency-space domain where integrations have been involved so that it might produce more stable results in practice.

1.3 Overview of the dissertation

After introducing the background for seismic exploration in Chapter 1, Chapter 2 will provide the theory of the deghosting algorithm explored in this dissertation. Derivations of closely related algorithms such as wavelet estimation and field prediction will also be presented. Advantages and limitations of the deghosting algorithm in this dissertation compared to other algorithms will also be discussed in Chapter 2.

Chapter 3 provides numerical tests of the deghosting algorithm and the ISS free surface multiple removal method is applied to the deghosted data. Numerical tests using receiver

array data will be presented too. Deghosting results are given when there is a small error in the depth of the streamers. The deghosting algorithm is also applied to ocean bottom data.

Chapter 4 provides a summary of this dissertation.

2. THEORY

In this chapter, I will present the theory of the deghosting method developed in this dissertation. Derivations of two other closely-related algorithms, source wavelet estimation and wavefield prediction, are also presented and discussed. I start from Green's Theorem, from which all of the three algorithms above can be derived. After the derivations, the assumptions, limitations, and advantages for each algorithm will be discussed.

Before getting into the mathematics, I would like to explain some seismic terms that are going to be used. This dissertation mainly focuses on offshore applications, hence the words "field" or "wavefield" mean the pressure measured by hydrophones in the water. On-shore activities use geophone measurements which correspond to the velocity of the medium particles. The terms "wavelet", "source wavelet", or "source signature" denote the way the source vibrates. Different data will be recorded if different source wavelet is used. However, the subsurface properties are totally independent of the source wavelet. So it is important to figure out in what way the source vibrates so that its effect on the data can be removed and the real subsurface response can be extracted. "Reference wave" is used to describe waves travel only in the reference medium (water) without being reflected by the earth. Because of the free surface (air-water interface), the reference wave includes two parts. One is called the direct wave (G_0^d), which travels directly from the source to the receiver; the other is the ghost of the direct wave (G_0^{FS}) which travels up from the source to the free surface and then reflected back to the receivers (Weglein *et al.*, 2003). "Scattered wave" represents all waves that have been reflected by the earth. It can also be separated into two

parts: those moving *upward* to the receivers and those moving *downward* to the receivers.

I start from Green's Theorem (Green's Second Identity):

$$\int_V \left(\psi(\mathbf{r}', \mathbf{r}_s, \omega)\nabla'^2\phi(\mathbf{r}', \mathbf{r}, \omega) - \phi(\mathbf{r}', \mathbf{r}, \omega)\nabla'^2\psi(\mathbf{r}', \mathbf{r}_s, \omega)\right) d\mathbf{r}' = \oint_S \left[\psi(\mathbf{r}', \mathbf{r}_s, \omega)\nabla'\phi(\mathbf{r}', \mathbf{r}, \omega) - \phi(\mathbf{r}', \mathbf{r}, \omega)\nabla'\psi(\mathbf{r}', \mathbf{r}_s, \omega)\right] \cdot d\mathbf{S}', \tag{2.1}$$

where $\psi(\mathbf{r}', \mathbf{r}_s, \omega)$ and $\phi(\mathbf{r}', \mathbf{r}, \omega)$ are two arbitrary functions chosen such that their second derivative and the integrations in Eq. 2.1 exist. The surface S encloses volume V. In this dissertation, $\psi(\mathbf{r}', \mathbf{r}_s, \omega)$ is associated with the pressure wavefield in the actual medium $P(\mathbf{r}', \mathbf{r}_s, \omega)$, which is assumed to satisfy the acoustic wave equation

$$\nabla'^2 P(\mathbf{r}', \mathbf{r}_s, \omega) + \frac{\omega^2}{c^2(\mathbf{r}')} P(\mathbf{r}', \mathbf{r}_s, \omega) = A(\omega)\delta(\mathbf{r}' - \mathbf{r}_s) \tag{2.2}$$

in the volume V, where $A(\omega)$ is the source wavelet. I will consider the whole space in a perturbative way. The background is a whole space of water, then there is a perturbation $\alpha(\mathbf{r}')$ added to the background to change water into air by α_{air} and change water into earth by α_{earth}. Substituting $\frac{\omega^2}{c^2(\mathbf{r}')}$ with $k_0^2(1 - \alpha(\mathbf{r}'))$ where $k_0^2 = \frac{\omega^2}{c_0^2}$, Eq. 2.2 becomes

$$\begin{aligned} \nabla'^2 P(\mathbf{r}', \mathbf{r}_s, \omega) + k_0^2 P(\mathbf{r}', \mathbf{r}_s, \omega) &= A(\omega)\delta(\mathbf{r}' - \mathbf{r}_s) + k_0^2\alpha(\mathbf{r}')P(\mathbf{r}', \mathbf{r}_s, \omega) \\ &= A(\omega)\delta(\mathbf{r}' - \mathbf{r}_s) + k_0^2\left(\alpha_{air}(\mathbf{r}') + \alpha_{earth}(\mathbf{r}')\right) P(\mathbf{r}', \mathbf{r}_s, \omega) \end{aligned} \tag{2.3}$$

where $\alpha(\mathbf{r}')$ represents the difference between the actual and reference medium and consists of two parts $\alpha_{air}(\mathbf{r}')$ and $\alpha_{earth}(\mathbf{r}')$ which, respectively, denote the difference between air and water and earth and water.

In the following, it will be shown that different algorithms can be derived by choosing a

different volume V, a different position of $\mathbf{r}_s$ and replacing function $\phi(\mathbf{r}', \mathbf{r}, \omega)$ in Eq. 2.1 by a different Green's function in the reference medium (water) with different boundary conditions.

2.1 Derivation of the wavelet estimation formula (Weglein and Secrest, 1990)

This time, I replace $\phi(\mathbf{r}', \mathbf{r}, \omega)$ with the Green's function $G_0^D(\mathbf{r}', \mathbf{r}, \omega)$ in the half space reference medium which satisfies

$$\nabla'^2 G_0^D(\mathbf{r}', \mathbf{r}, \omega) + k_0^2 G_0^D(\mathbf{r}', \mathbf{r}, \omega) = \delta(\mathbf{r}' - \mathbf{r}) - \delta(\mathbf{r}' - \mathbf{r}_I), \tag{2.4}$$

where $\mathbf{r}_I$ is the mirror image of $\mathbf{r}$ with respect to the free surface. The minus sign before the second delta function is due to the polarity change after the wave is reflected by the free surface. Substituting Eq. 2.4 and Eq. 2.3 into Eq. 2.1 provides

$$\begin{aligned}
&\int_V \Big(P(\mathbf{r}', \mathbf{r}_s, \omega) \nabla'^2 G_0^D(\mathbf{r}', \mathbf{r}, \omega) - G_0^D(\mathbf{r}', \mathbf{r}, \omega) \nabla'^2 P(\mathbf{r}', \mathbf{r}_s, \omega) \Big) \, d\mathbf{r}' \\
&= \int_V P(\mathbf{r}', \mathbf{r}_s, \omega) \Big(\delta(\mathbf{r}' - \mathbf{r}) - \delta(\mathbf{r}' - \mathbf{r}_I) - k_0^2 G_0^D(\mathbf{r}', \mathbf{r}, \omega) \Big) d\mathbf{r}' \\
&- \int_V G_0^D(\mathbf{r}', \mathbf{r}, \omega) \Big(A(\omega) \delta(\mathbf{r}' - \mathbf{r}_s) + k_0^2 \left(\alpha_{air}(\mathbf{r}') + \alpha_{earth}(\mathbf{r}') \right) P(\mathbf{r}', \mathbf{r}_s, \omega) - k_0^2 P(\mathbf{r}', \mathbf{r}_s, \omega) \Big) \, d\mathbf{r}' \\
&= \oint_S \left[P(\mathbf{r}', \mathbf{r}_s, \omega) \nabla' G_0^D(\mathbf{r}', \mathbf{r}, \omega) - G_0^D(\mathbf{r}', \mathbf{r}, \omega) \nabla' P(\mathbf{r}', \mathbf{r}_s, \omega) \right] \cdot d\mathbf{S}'.
\end{aligned} \tag{2.5}$$

Now, choosing the half space below the measurement surface as V, and choosing $\mathbf{r}$ at a point below the measurement surface (inside of V) (Figure 2.1), Eq. 2.5 becomes

$$P(\mathbf{r}, \mathbf{r}_s, \omega) - \int_V G_0^D(\mathbf{r}', \mathbf{r}, \omega) k_0^2 \alpha_{earth}(\mathbf{r}') P(\mathbf{r}', \mathbf{r}_s, \omega) d\mathbf{r}'$$

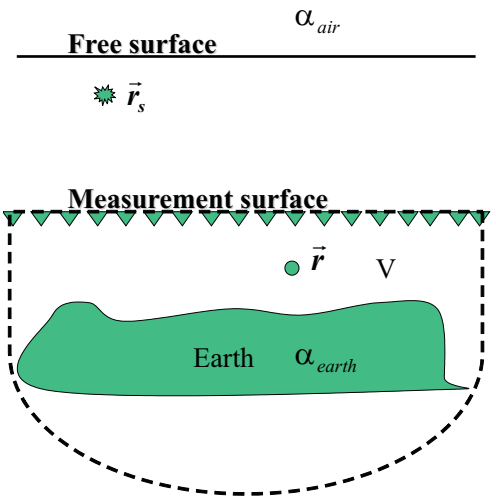

Fig. 2.1: *First configuration for derivation of the wavelet estimation algorithm.*

$$= \oint_S \left[P(\mathbf{r}', \mathbf{r}_s, \omega) \nabla' G_0^D(\mathbf{r}', \mathbf{r}, \omega) - G_0^D(\mathbf{r}', \mathbf{r}, \omega) \nabla' P(\mathbf{r}', \mathbf{r}_s, \omega) \right] \cdot d\mathbf{S}'. \qquad (2.6)$$

The physical meaning of each term in Eq. 2.6 needs to be analyzed in order to interpret Eq. 2.6. The term $P(\mathbf{r}, \mathbf{r}_s, \omega)$ on the LHS of Eq. 2.6 represents the total wavefield recorded at position $\mathbf{r}$ as shown in Fig. 2.1. The total field $P(\mathbf{r}, \mathbf{r}_s, \omega)$ can be regarded as the summation of the reference wavefield (which has *not* been reflected by the earth) and the scattered field (which has been reflected by the earth). Then the LHS of Eq. 2.6 will be the reference wavefield ($A(\omega)G_0^D(\mathbf{r}, \mathbf{r}_s, \omega)$), as long as I can prove the volume V integration in Eq. 2.6 is the scattered field. The volume integration is the scattered field, if the Green's function $G_0^D(\mathbf{r}', \mathbf{r}, \omega)$ is replaced by the causal Green's function in a whole space of water ($G_0^+(\mathbf{r}', \mathbf{r}, \omega)$) when there is no free surface. However, due to the existence of the free surface, $G_0^D(\mathbf{r}', \mathbf{r}, \omega)$ is needed to construct part of the scattered wave that travels up to the free surface then reflected down to the receiver. So the volume integration in Eq. 2.6 is the total scattered field when there is a free surface. Hence, the source wavelet estimation equation (Weglein

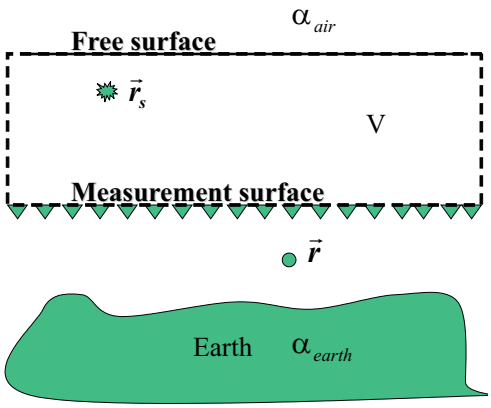

Fig. 2.2: Second configuration for derivation of the wavelet estimation algorithm.

and Secrest, 1990) is obtained:

$$A(\omega) \quad G_0^D(\mathbf{r}, \mathbf{r}_s, \omega) = \oint_S \left[P(\mathbf{r}', \mathbf{r}_s, \omega)\nabla' G_0^D(\mathbf{r}', \mathbf{r}, \omega) - G_0^D(\mathbf{r}', \mathbf{r}, \omega)\nabla' P(\mathbf{r}', \mathbf{r}_s, \omega)\right] \cdot d\mathbf{S}' \quad (2.7)$$

$$= \int_{m.s.} \left[P(\mathbf{r}', \mathbf{r}_s, \omega)\nabla' G_0^D(\mathbf{r}', \mathbf{r}, \omega) - G_0^D(\mathbf{r}', \mathbf{r}, \omega)\nabla' P(\mathbf{r}', \mathbf{r}_s, \omega)\right] \cdot d\mathbf{S}', \quad (2.8)$$

where at the last step, the properties of $P(\mathbf{r}', \mathbf{r}_s, \omega)$ and $G_0^D(\mathbf{r}', \mathbf{r}, \omega)$ at the free surface have been used and m.s. denotes the measurement surface.

Another way of deriving Eq. 2.8 is to start from Eq. 2.5, and choose the space between the free surface and the measurement surface as volume V (Figure 2.2). Then Eq. 2.8 can be directly obtained since all sources are outside of V, except the active source $\delta(\mathbf{r}' - \mathbf{r}_s)$.

Discussion

1. Weglein and Secrest (1990) used a different approach to obtain this algorithm and demonstrated that in the more general case of an unknown source array, instead of point source, it can provide the reference wave field in the volume below the measurement surface.

2. Eq. 2.8 is an expression of the so-called triangle relationship among pressure P, its vertical derivative $\frac{dP}{dz}$ and the source wavelet $A(\omega)$. Knowing any two of these quantities, the third one can be calculated. As seen later in this dissertation, this relationship is used to calculate the vertical derivative of P for ocean bottom deghosting.

3. Using conventional towed streamer measurements where only pressure P is available, Eq. 2.8 cannot be applied directly since Eq. 2.8 requires both pressure and its derivative. New advances in seismic acquisition technology (Carlson *et al.*, 2007; Moldoveanu *et al.*, 2007) that measure both P and its vertical derivative provide a good opportunity for the direct application of this algorithm. It is important to note that for most cases, data at small offsets (less than $100m$ or $200m$) are usually not measured. As simple numerical tests demonstrates that the measurements at these small offsets might be very important for this wavelet estimation algorithm.

   The numerical test model is shown in Fig. 2.3 where the source is at $(0, 2m)$ and receivers are at depth $6m$. The medium is a whole space of water, i.e., is modeled as an acoustic, constant density medium with a wave speed of $1500m/s$. The evaluation point can be anywhere below the measurement surface and in principle, the same source wavelet (-1) is supposed to be obtained. In Fig. 2.4, the calculated source wavelets are shown for the evaluation points are at depth $8m$ with offsets ranging from $0m$ to $2000m$. When the data at small offset is not missing, a very consistent and accurate wavelet is obtained. However, if the data at offsets less than $200m$ are missing, then the results contain significant error. Fig. 2.5 shows the results when the evaluation points are at $200m$ depth. Again, very good results are obtained when there is no missing small offset data, while significant error occurs when the small offset measurements are missed.

   Fig. 2.6 explains why this happens. The integrand of the integration term in Eq. 2.8 is plotted in Fig. 2.6 for the case that the evaluation point is at $(1000m, 200m)$.

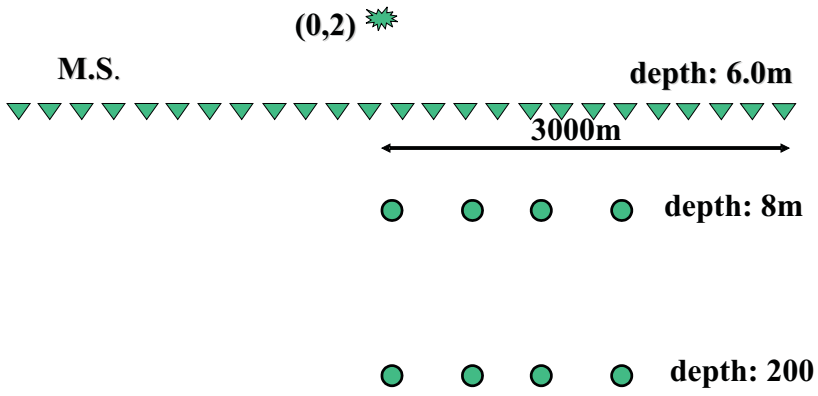

Fig. 2.3: *Configuration for testing of missing offsets measurements on Green's Theorem wavelet estimation algorithm.*

Obviously, the integrand at small offsets ($< 200m$) is large and missing its contribution will cause significant error in the integration result. Fig. 2.6 suggests where the closest offset receiver needs to be in order to be able to effectively extrapolate and allow Eq. 2.8 to be effective, for the case that the effect of scattered field is negligible at small offsets.

2.2 *Derivation of the field prediction formula (Osen* et al.*, 1998; Tan, 1999; Weglein* et al.*, 2000)*

Consider again Eq. 2.1, I replace $\phi(\mathbf{r}', \mathbf{r}, \omega)$ with the Green's function $G_0^{DD}(\mathbf{r}', \mathbf{r}, \omega)$ [1] in whole space reference medium (water) which satisfies

$$\nabla'^2 G_0^{DD}(\mathbf{r}', \mathbf{r}, \omega) + k_0^2 G_0^{DD}(\mathbf{r}', \mathbf{r}, \omega) = \delta(\mathbf{r}' - \mathbf{r}) + \sum_{i=1}^{\infty} a_i \delta(\mathbf{r}' - \mathbf{r}_i), \tag{2.9}$$

[1] "DD" stands for the "double Dirichlet" bounary condition

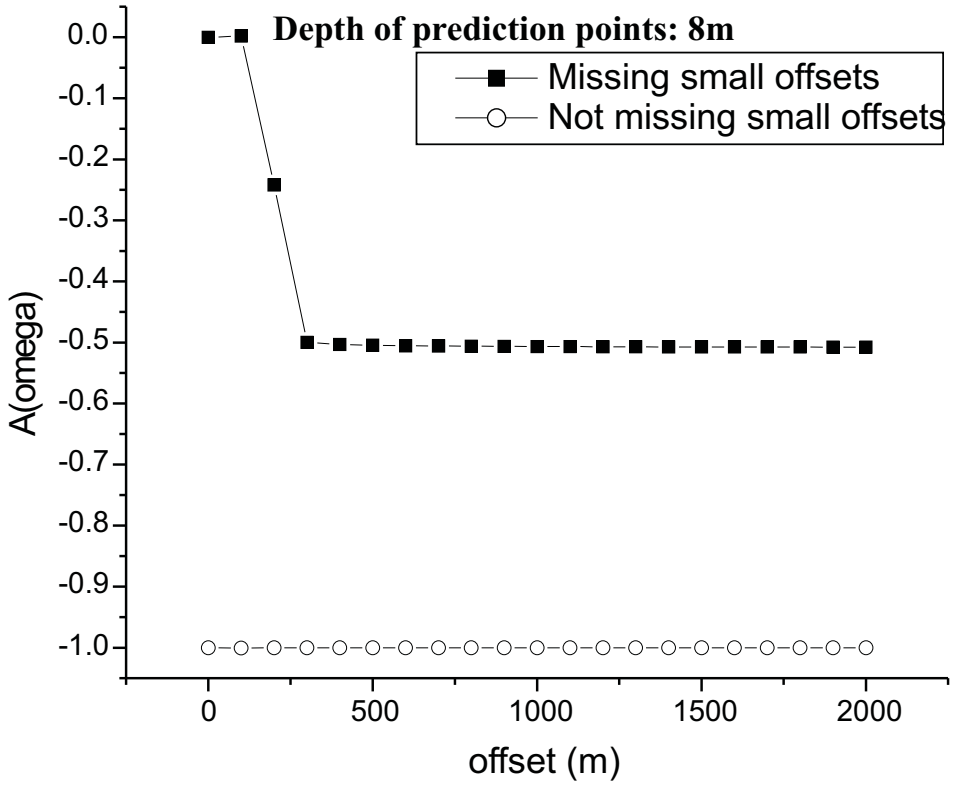

Fig. 2.4: *Effects of small offset measurements on the Green's Theorem wavelet estimation algorithm. Depth of the evaluation points is* $8.0m$. *The exact value of the source wavelet is* -1.0.

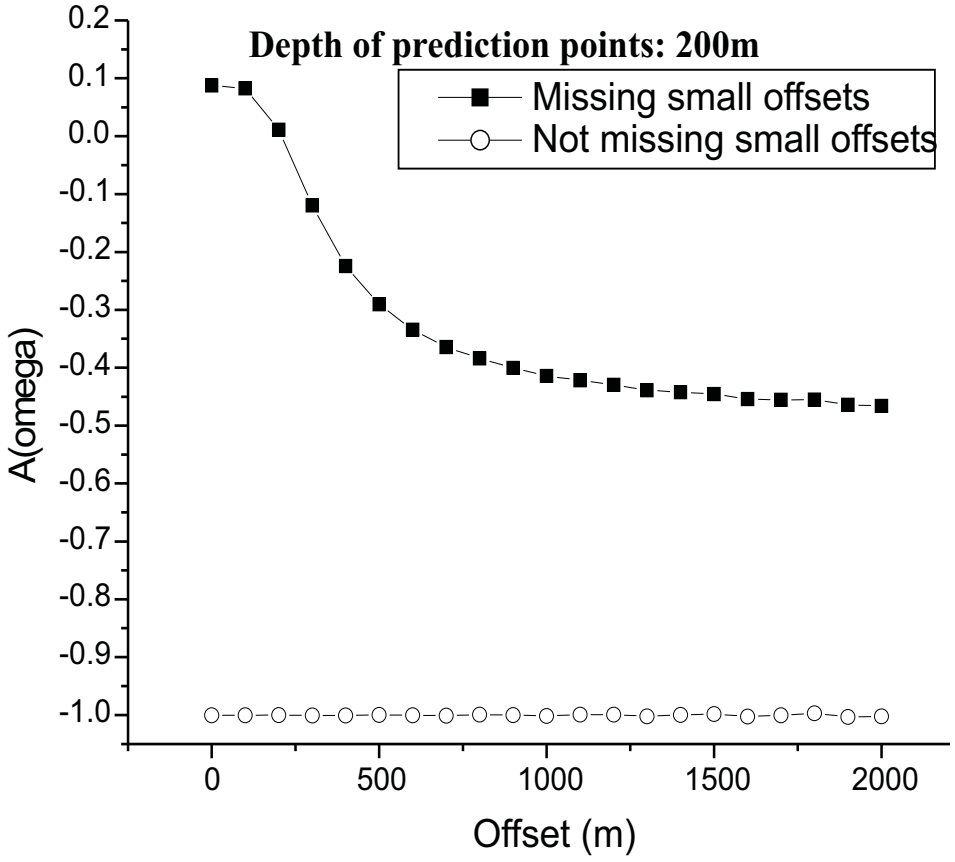

Fig. 2.5: *Effects of small offset measurements on the Green's Theorem wavelet estimation algorithm. Depth of the evaluation points is* $200.0m$. *The exact value of the source wavelet is* -1.0.

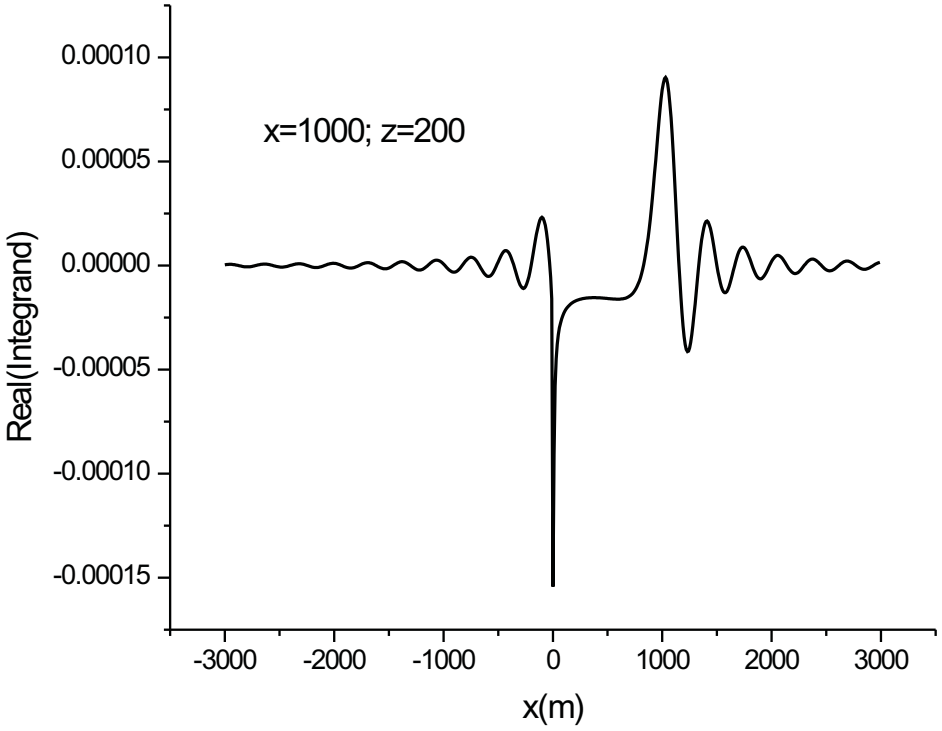

Fig. 2.6: *Integrand of the integration term in Eq. 2.8 when the evaluation point is at* $(1000m, 200m)$. *Contributions of data at small offsets are important for the proper integration value.*

where $\mathbf{r}_i$, for $i = 1, 2, 3, \ldots$ is the position of one of the infinite number of mirror images of $\mathbf{r}$ with respect to the free surface and the measurement surface. This ensures that the resulting G_0^{DD} vanishes at both surfaces which for reasons shown below is a useful property. Coefficient a_i can be positive or negative 1. Then substituting Eq. 2.9 and Eq. 2.3 into Eq. 2.1 provides

$$\begin{aligned}
&\int_V \Big(P(\mathbf{r}', \mathbf{r}_s, \omega) \nabla'^2 G_0^{DD}(\mathbf{r}', \mathbf{r}, \omega) - G_0^{DD}(\mathbf{r}', \mathbf{r}, \omega) \nabla'^2 P(\mathbf{r}', \mathbf{r}_s, \omega) \Big) \, d\mathbf{r}' \\
&= \int_V P(\mathbf{r}', \mathbf{r}_s, \omega) \Big(\delta(\mathbf{r}' - \mathbf{r}) + \sum_{i=1}^{\infty} a_i \delta(\mathbf{r}' - \mathbf{r}_i) - k_0^2 G_0^{DD}(\mathbf{r}', \mathbf{r}, \omega) \Big) d\mathbf{r}' \\
&- \int_V G_0^{DD}(\mathbf{r}', \mathbf{r}, \omega) \Big(A(\omega) \delta(\mathbf{r}' - \mathbf{r}_s) + k_0^2 \left(\alpha_{air}(\mathbf{r}') + \alpha_{earth}(\mathbf{r}') \right) P(\mathbf{r}', \mathbf{r}_s, \omega) - k_0^2 P(\mathbf{r}', \mathbf{r}_s, \omega) \Big) \, d\mathbf{r}' \\
&= \oint_S \left[P(\mathbf{r}', \mathbf{r}_s, \omega) \nabla' G_0^{DD}(\mathbf{r}', \mathbf{r}, \omega) - G_0^{DD}(\mathbf{r}', \mathbf{r}, \omega) \nabla' P(\mathbf{r}', \mathbf{r}_s, \omega) \right] \cdot d\mathbf{S}'. \qquad (2.10)
\end{aligned}$$

Now, choosing the space between the free surface and the measurement surface as V, and putting $\mathbf{r}$ anywhere inside V (Figure 2.7), Eq. 2.10 becomes the field prediction equation (Osen *et al.*, 1998; Tan, 1999; Weglein *et al.*, 2000)

$$\begin{aligned}
P(\mathbf{r}, \mathbf{r}_s, \omega) =& A(\omega) G_0^{DD}(\mathbf{r}, \mathbf{r}_s, \omega) \\
&+ \oint_S \left[P(\mathbf{r}', \mathbf{r}_s, \omega) \nabla' G_0^{DD}(\mathbf{r}', \mathbf{r}, \omega) - G_0^{DD}(\mathbf{r}', \mathbf{r}, \omega) \nabla' P(\mathbf{r}', \mathbf{r}_s, \omega) \right] \cdot d\mathbf{S}', \qquad (2.11) \\
=& A(\omega) G_0^{DD}(\mathbf{r}, \mathbf{r}_s, \omega) + \int_{m.s.} P(\mathbf{r}', \mathbf{r}_s, \omega) \nabla' G_0^{DD}(\mathbf{r}', \mathbf{r}, \omega) \cdot d\mathbf{S}', \qquad (2.12)
\end{aligned}$$

where at the last step the properties of $P(\mathbf{r}', \mathbf{r}_s, \omega)$ and $G_0^{DD}(\mathbf{r}', \mathbf{r}, \omega)$ on the surfaces are used. Osen *et al.* (1998) regards the equation above as a wavelet estimation. The requirement is knowing the field ($P(\mathbf{r}', \mathbf{r}_s, \omega)$) on the measurement surface and one extra hydrophone measurement ($P(\mathbf{r}, \mathbf{r}_s, \omega)$) at any position between the free surface and the measurement surface. Then, the only unknown variable in Eq. 2.12 is the source wavelet $A(\omega)$, which may be solved for.

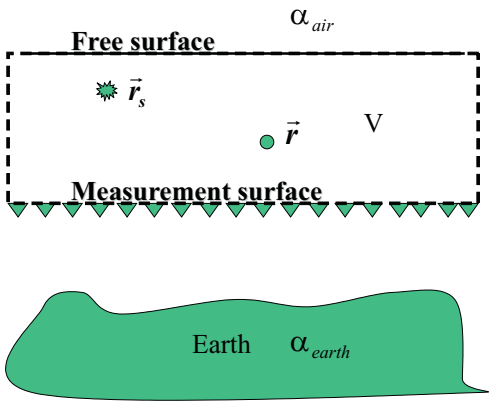

Fig. 2.7: Configuration for derivation of the field prediction algorithm.

Discussion

1. Eq. 2.12 provides the total wavefield at position $\mathbf{r}$ which can be anywhere between the free surface and the measurement surface, as long as the pressure measurements and the source wavelet are available. Taking the derivative with respect to z on both sides of Eq. 2.12 produces:

$$\frac{\partial P(\mathbf{r},\mathbf{r}_s,\omega)}{\partial z} = A(\omega)\frac{\partial}{\partial z}G_0^{DD}(\mathbf{r},\mathbf{r}_s,\omega) + \int_{m.s.} P(\mathbf{r}',\mathbf{r}_s,\omega)\nabla'\frac{\partial}{\partial z}G_0^{DD}(\mathbf{r}',\mathbf{r},\omega)\cdot d\mathbf{S}', \tag{2.13}$$

   which can be used to calculate the vertical derivative of P.

2. G_0^{DD} is a purely mathematical function which vanishes both at the free surface and the measurement surface. Its derivation can be found in Tan (1999). A different derivation is provided in Appendix B. G_0^{DD} has a special property: it will decay exponentially as offset $|x - x_s|$ (for the 2D case) increases, for frequencies less than $125Hz$, if the depth of the streamer is $6.0m$ and water wave velocity is $1500.0m/s$ (See details in Appendix B). The values of $G_0^{DD}(x, z = 5.9m, x_s = 0, z_s = 2.0m)$ for

three different frequencies is plotted against offset x in Fig. 2.8, assuming the depth of the measurement surface is 6.0m and the depth of the field prediction points is $5.9m$, i.e., $10cm$ above the measurement surface. If the depth of the prediction points are kept always $10cm$ above the measurement suface, then Fig. 2.9 provides the function value of $G_0^{DD}(x, x_s = 0, z_s = 2.0m, f = 25Hz)$ for three different measurement surface depths: $6m$, $15m$ and $20m$. For all cases, G_0^{DD} decays to zero very rapidly as offset increases.

There are two consequences of this rapid decay property. The first one is that the contributions of the source wavelet term in both Eq. 2.12 and Eq. 2.13 is negligible for big enough offsets ($|x - x_s| > 30m$ for all of the above mentioned parameters). Hence, for most of the offsets, the field P and its vertical derivative *can* be predicted even *without* the source wavelet. Thus, the following approximations can be obtained:

$$P(\mathbf{r}, \mathbf{r}_s, \omega) \approx \int_{m.s.} P(\mathbf{r}', \mathbf{r}_s, \omega) \tfrac{\partial}{\partial z'} G_0^{DD}(\mathbf{r}', \mathbf{r}, \omega) \cdot d\mathbf{S}' \tag{2.14}$$

$$\frac{\partial P(\mathbf{r}, \mathbf{r}_s, \omega)}{\partial z} \approx \int_{m.s.} P(\mathbf{r}', \mathbf{r}_s, \omega) \nabla' \tfrac{\partial}{\partial z} G_0^{DD}(\mathbf{r}', \mathbf{r}, \omega) \cdot d\mathbf{S}'. \tag{2.15}$$

Based on these two approximations, an early attempt at deghosting tried to perform deghosting only using the field measurements on the m.s. (Weglein *et al.*, 2002). It has been found that using these two approximations, the direct wave and its ghosts cannot be removed. The scattered field, however, can be deghosted very well. The reason is that although Eq. 2.14 and Eq. 2.15 are approximations for the *total* wavefield at position $\mathbf{r}$, they are actually *exact* equations for the *scattered* field. That is, for the scattered field P_s,

$$P_s(\mathbf{r}, \mathbf{r}_s, \omega) = \int_{m.s.} P_s(\mathbf{r}', \mathbf{r}_s, \omega) \tfrac{\partial}{\partial z'} G_0^{DD}(\mathbf{r}', \mathbf{r}, \omega) \cdot d\mathbf{S}', \tag{2.16}$$

$$\frac{\partial P_s(\mathbf{r}, \mathbf{r}_s, \omega)}{\partial z} = \int_{m.s.} P_s(\mathbf{r}', \mathbf{r}_s, \omega) \nabla' \tfrac{\partial}{\partial z} G_0^{DD}(\mathbf{r}', \mathbf{r}, \omega) \cdot d\mathbf{S}', \tag{2.17}$$

which can be derived using Green's Theorem by replacing the total field P by the scattered field P_s that satisfies:

$$\nabla'^2 P_s(\mathbf{r}', \mathbf{r}_s, \omega) + \frac{\omega^2}{c^2(\mathbf{r}')} P_s(\mathbf{r}', \mathbf{r}_s, \omega) = 0. \tag{2.18}$$

Notice that compared to the total wavefield Eq. 2.2, there is no source term for the scattered field. Eq. 2.16 and Eq. 2.17 make perfect sense in terms of Green's Theorem: "Given the field information on the surface and the medium information inside the volume, the wavefield anywhere in the volume can be calculated." (See Appendix A). For the scattered field, there is no source between the m.s. and the free surface, so knowing the field on the m.s. is enough to determine the scattered field anywhere between the free surface and the m.s.. Next replacing the total wavefield (P) by the summation of the reference wavefield (P_0) and the scattered wavefield (P_s), Eq. 2.14 becomes

$$\begin{aligned} P(\mathbf{r}, \mathbf{r}_s, \omega) &\approx \int_{m.s.} P(\mathbf{r}', \mathbf{r}_s, \omega) \frac{\partial}{\partial z'} G_0^{DD}(\mathbf{r}', \mathbf{r}, \omega) \cdot d\mathbf{S}' \\ &\approx \int_{m.s.} (P_0(\mathbf{r}', \mathbf{r}_s, \omega) + P_s(\mathbf{r}', \mathbf{r}_s, \omega)) \frac{\partial}{\partial z'} G_0^{DD}(\mathbf{r}', \mathbf{r}, \omega) \cdot d\mathbf{S}' \\ &\approx \int_{m.s.} P_0(\mathbf{r}', \mathbf{r}_s, \omega) \frac{\partial}{\partial z'} G_0^{DD}(\mathbf{r}', \mathbf{r}, \omega) \cdot d\mathbf{S}' + P_s(\mathbf{r}, \mathbf{r}_s, \omega) \end{aligned} \tag{2.19}$$

where at the last step, Eq. 2.16 has been used. At the same time, the total wavefield on the LHS is the summation of two P_0 and P_S. The scattered field P_s cancels on both sides. So Eq. 2.19 and Eq. 2.14 are actually approximations for the reference wavefield P_0. The source wavelet terms in Eq. 2.12 and Eq. 2.13 only contribute to the reference wavefield and its derivative. This is the reason why using the wavefield on the m.s. only can still deghost the scattered field, while the reference wavefield can not be removed.

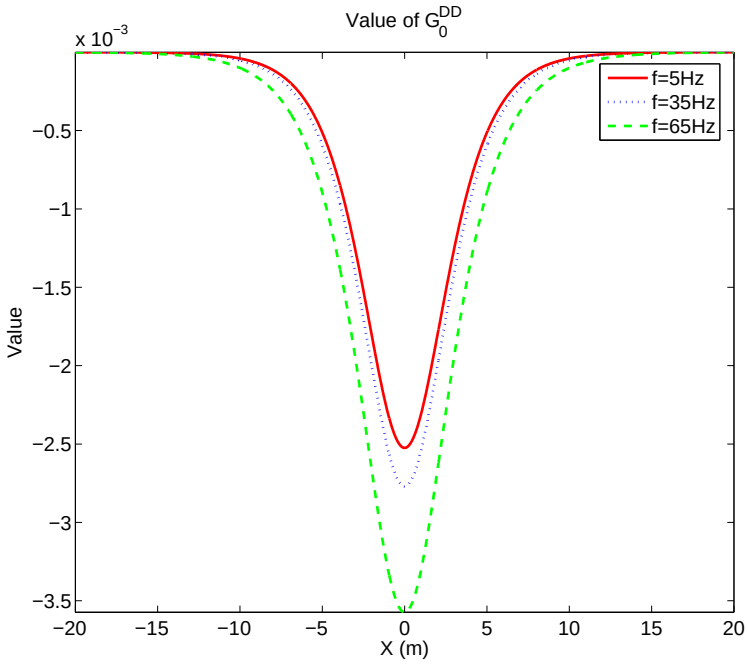

Fig. 2.8: G_0^{DD} *for three different frequencies.*

The other consequence of the property of G_0^{DD} is that, although the integration term in Eq. 2.12 and Eq. 2.13 requires the field from $-\infty$ to $+\infty$, only a small region of field on the m.s. (close to the prediction point $\mathbf{r}$) contributes significantly. This interesting feature will be discussed later in the deghosting section.

2.3 Derivation of the deghosting algorithm (Weglein et al.*, 2002)*

Consider again Eq. 2.1, substituting for $\phi(\mathbf{r}', \mathbf{r}, \omega)$ with the causal Green's function $G_0^+(\mathbf{r}', \mathbf{r}, \omega)$ in the whole space reference medium which satisfies

$$\nabla'^2 G_0^+(\mathbf{r}', \mathbf{r}, \omega) + k_0^2 G_0^+(\mathbf{r}', \mathbf{r}, \omega) = \delta(\mathbf{r}' - \mathbf{r}), \tag{2.20}$$

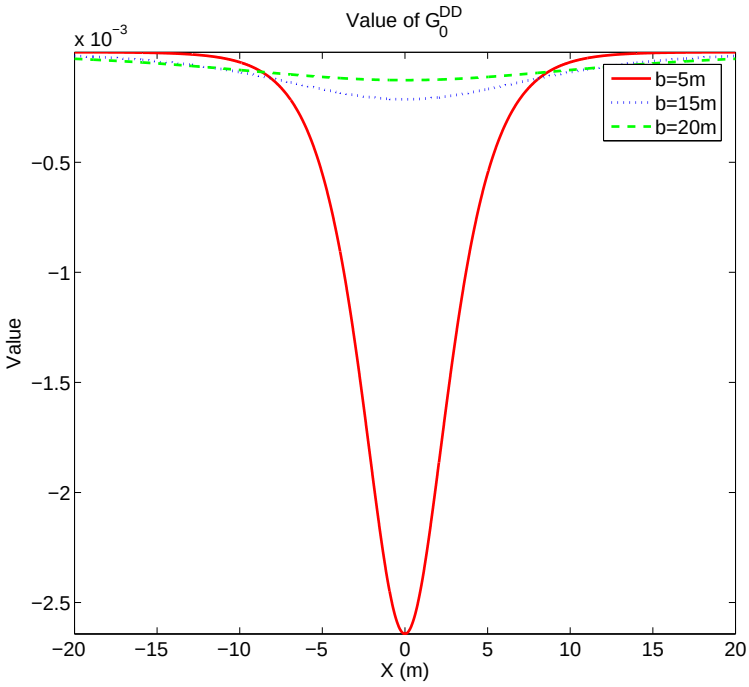

Fig. 2.9: G_0^{DD} *for three different depths.*

then substituting Eq. 2.20 and Eq. 2.3 into Eq. 2.1 provide

$$\begin{aligned}
&\int_V \Big(P(\mathbf{r}',\mathbf{r}_s,\omega)\nabla'^2 G_0^+(\mathbf{r}',\mathbf{r},\omega) - G_0^+(\mathbf{r}',\mathbf{r},\omega)\nabla'^2 P(\mathbf{r}',\mathbf{r}_s,\omega)\Big)\, d\mathbf{r}' \\
&= \int_V P(\mathbf{r}',\mathbf{r}_s,\omega)\Big(\delta(\mathbf{r}'-\mathbf{r}) - k_0^2 G_0^+(\mathbf{r}',\mathbf{r},\omega)\Big) d\mathbf{r}' \\
&- \int_V G_0^+(\mathbf{r}',\mathbf{r},\omega)\Big(A(\omega)\delta(\mathbf{r}'-\mathbf{r}_s) + k_0^2\left(\alpha_{air}(\mathbf{r}') + \alpha_{earth}(\mathbf{r}')\right)P(\mathbf{r}',\mathbf{r}_s,\omega) - k_0^2 P(\mathbf{r}',\mathbf{r}_s,\omega)\Big)\, d\mathbf{r}' \\
&= \oint_S \left[P(\mathbf{r}',\mathbf{r}_s,\omega)\nabla' G_0^+(\mathbf{r}',\mathbf{r},\omega) - G_0^+(\mathbf{r}',\mathbf{r},\omega)\nabla' P(\mathbf{r}',\mathbf{r}_s,\omega)\right]\cdot d\mathbf{S}'. \qquad (2.21)
\end{aligned}$$

Choosing the half space above the measurement surface to be V, and putting $\mathbf{r}$ anywhere between the free surface and the measurement surface (inside of V) (Figure 2.10), Eq. 2.21 becomes

$$P(\mathbf{r},\mathbf{r}_s,\omega) - A(\omega)G_0^+(\mathbf{r},\mathbf{r}_s,\omega) - \int_V G_0^+(\mathbf{r}',\mathbf{r},\omega)k_0^2\alpha_{air}(\mathbf{r}')P(\mathbf{r}',\mathbf{r}_s,\omega)d\mathbf{r}'$$

$$= \oint_S \left[P(\mathbf{r}', \mathbf{r}_s, \omega) \nabla' G_0^+(\mathbf{r}', \mathbf{r}, \omega) - G_0^+(\mathbf{r}', \mathbf{r}, \omega) \nabla' P(\mathbf{r}', \mathbf{r}_s, \omega) \right] \cdot d\mathbf{S}', \qquad (2.22)$$

where α_{air} denotes the difference between the air and water. The physical meaning of Eq. 2.22 is as follows. The total wavefield at point $\mathbf{r}$ can be separated into three parts: (1) the direct wave which travels from the source to $\mathbf{r}$, (2) the field whose last motion is *downward* from the free surface and (3) the field whose last motion is *upward* from the earth. In Eq. 2.22 the term that contains the source wavelet is part (1) and the volume integration term is part (2). Therefore, the whole LHS of Eq. 2.22 corresponds to part (3), the up-going (or the receiver side deghosted) wavefield at point $\mathbf{r}$. Thus, the deghosting algorithm is derived:

$$P^{deghosted}(\mathbf{r}, \mathbf{r}_s, \omega) = \oint_S \left[P(\mathbf{r}', \mathbf{r}_s, \omega) \nabla' G_0^+(\mathbf{r}', \mathbf{r}, \omega) - G_0^+(\mathbf{r}', \mathbf{r}, \omega) \nabla' P(\mathbf{r}', \mathbf{r}_s, \omega) \right] \cdot d\mathbf{S}' \quad (2.23)$$

$$= \int_{m.s.} \left[P(\mathbf{r}', \mathbf{r}_s, \omega) \nabla' G_0^+(\mathbf{r}', \mathbf{r}, \omega) - G_0^+(\mathbf{r}', \mathbf{r}, \omega) \nabla' P(\mathbf{r}', \mathbf{r}_s, \omega) \right] \cdot d\mathbf{S}', \quad (2.24)$$

where in the last step the Sommerfeld Radiation condition eliminates the upper half space contribution at infinite distance.

Eq. 2.24 can be easily understood if the idea of Extinction Theorem (Born and Wolf, 1999) is used, which is an interpretation of the Green's Theorem with a *causal* Green's function. In optics, the name Extinction Theorem is used to emphasize one of the amazing properties of the surface integration term in Green's theorem: if a causal $P(\mathbf{r}', \mathbf{r}, \omega)$ and a causal Green's function are used on the integration surface, then the surface integration term always produces the wavefield contributions due to sources inside (outside) of the volume, if the output point $\mathbf{r}$ is outside (inside) of V. In other words, the outside (inside) source contributions have been extinguished/eliminated. Another interesting property of the surface integration term will be mentioned later.

To derive Eq. 2.24 using the Extinction Theorem, the same volume V and position $\mathbf{r}$ can be chosen as above. Then, using a causal Green's function and according to the above

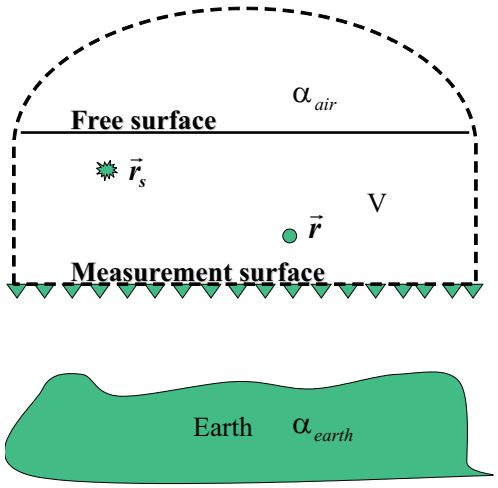

Fig. 2.10: *First configuration for derivation of the deghosting algorithm.*

mentioned property, the surface integration will eliminate wavefield contributions due to the source inside of V (which are the active source and the air) and only contributions due to source outside of V (which is the earth) will be kept. Since the wavefield due to the earth is up-going at $\mathbf{r}$, the surface integration term will produce the receiver side deghosted field.

Another way of using the Extinction Theorem to derive Eq. 2.24 is to choose the volume V as the half space below the measurement surface (Figure 2.11), with the position of $\mathbf{r}$ (outside of V) and the causal Green's function being the same as above. Then the surface integration will only keep the contribution due to the source inside of V, which is the earth. Hence, the integration provides the up-going, or receiver side deghosted wavefield.

Discussion

1. Eq. 2.24 requires both pressure and its vertical derivative to perform deghosting. Similar to the wavelet estimation algorithm mentioned above, new acquisition methods will provide an opportunity to directly apply this method. Performing deghosting

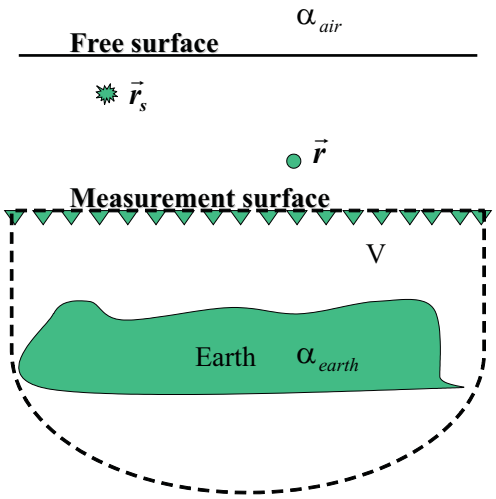

Fig. 2.11: *Second configuration for derivation of the deghosting algorithm.*

using conventional acquisition measurements, where only pressure measurements are available, is the goal of this dissertation. The method uses the pressure measurements on the m.s. to predict the pressure and its vertical derivative at a shallower depth, which I refer to as the pseudo m.s. (p.m.s.)(Fig. 2.12). Then since both pressure and its vertical derivative on the p.m.s. are available, deghosting can be performed using Eq. 2.24. The only question is: how to predict pressure and its vertical derivative. Here is where the field prediction algorithms Eq. 2.12 and Eq. 2.13 mentioned above are needed, which in turn means the source wavelet needs to be available. This availability is an assumption in all of the numerical tests on deghosting and free surface multiple removal in this dissertation.

As discussed before, if no estimate of the source wavelet is available, the field and its vertical derivative can be approximated using Eq. 2.14 and Eq. 2.15. The consequences of these approximations are that the reference wave can not be removed, while the scattered field can still be deghosted well. This residue of the reference

wave causes no problem if it does not overlap with the scattered field. At areas where the two waves overlap, the well deghosted scattered field will be compromised by the reference wave.

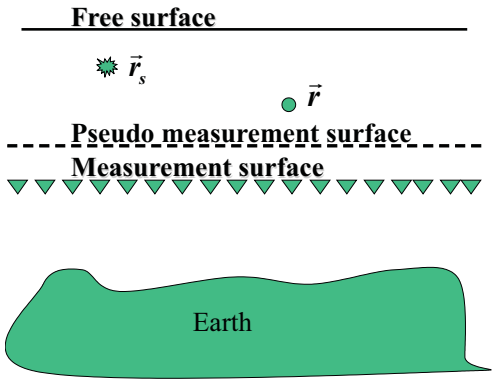

Fig. 2.12: *Field and its vertical derivative can be predicted on pseudo measurement surface using source wavelet and field measurements on m.s..*

2. Using Eq. 2.24 and the above scheme, the down-going wave on the receiver side (i.e., receiver ghosts) will be removed. Then a similar procedure is needed to remove source side ghosts (up-going wave on source side). To clearly explain how to perform source side deghosting, I would like to start from the beginning of the data acquisition. In a typical offshore seismic survey, a source is initiated and receivers at all offsets will receive the total wavefield (reference and scattered) for a certain length of time at their locations. The data set for all receivers due to *one* common source is called a common shot gather. Then the source is moved to a different location, usually at the same depth, and initiate again to obtain another common shot gather. For a $2D$ earth, sources need to be initiated everywhere (or, over a large enough distance to cover the area of interest), since each common shot gather is different (Fig. 2.13) from the others. For a $1.5D$ earth (which means the wave travels in two dimensions, while

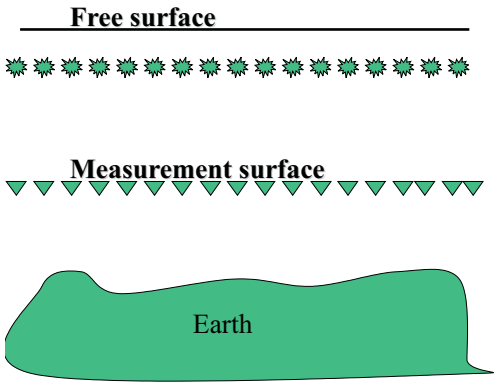

Fig. 2.13: *For 2D earth, sources and receivers need to be everywhere.*

the earth is $1D$), one shot gather is enough since each shot gather will be exactly the same as the others after a horizontal shift. After all of the data are received, they may be arranged in a certain order or transformed to a certain domain in order to be processed by different algorithms. The deghosting algorithm in Eq. 2.24 performs receiver side deghosting on data organized into a common shot gather (Fig. 2.14). Then, shot gather by shot gather, all of the receiver ghosts in the data are removed. After that, the data are then rearranged into common receiver gathers (data set for one fixed receiver due to all sources, Fig. 2.15). To directly apply Eq. 2.24, I change the receiver coordinate to a source coordinate and the sources to receivers in Fig. 2.15 to obtain Fig. 2.16. It is appropriate to make this change because of the theorem of wavefield reciprocity (Fokkema and van den Berg, 1993). Note that the common receiver gather data set in Fig. 2.15 is exactly the same as the common source gather in Fig. 2.16. Eq. 2.24 can be directly applied to the configuration in Fig. 2.16 to get rid of the original source ghosts.

3. For most conventional acquisition geometries where only pressure is measured, the deghosting scheme discussed above uses integration to predict pressure and its verti-

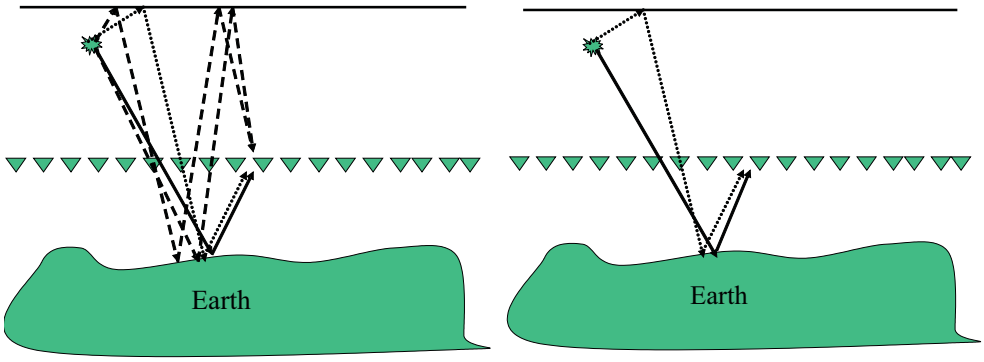

Fig. 2.14: *Receiver side deghosting works in common shot gather domain. Solid lines: primary; Dashed line: receiver ghost and source-receiver ghost; Dotted lines: source ghost. Left figure: Before deghosting (four events); Right figure: After receiver side deghosting (two events)*

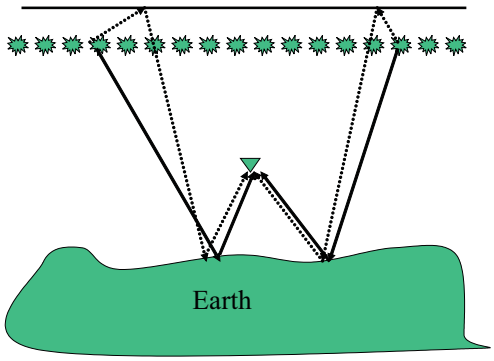

Fig. 2.15: *The data is arranged into common receiver gather before perform source side deghosting. Solid lines: primaries; Dotted lines: source ghosts*

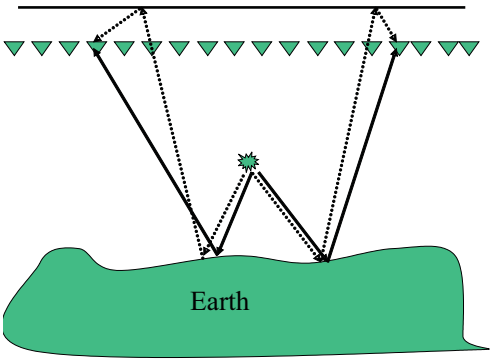

Fig. 2.16: *After switching the positions of source and receiver, Eq. 2.24 can be directly applied in this common source gather. Note that the original source ghosts in Fig. 2.15 become receiver ghosts.*

cal derivative. This approach can be advantageous in practice since integration is a process that is usually very stable and helps reduce random noise.

Also, the effect of the limited data aperture is small since as discussed above in the prediction of wavefield and its vertical derivative, G_0^{DD} decays exponentially as the horizontal distance between the prediction point and receivers on the cable increases. This again might be of some advantage compared to methods that try to obtain the vertical derivative of pressure through Fourier transforming the data into wavenumber domain (Amundsen *et al.*, 2005).

4. New receivers that measure both pressure and its vertical derivative provide an opportunity not only to directly apply this deghosting algorithm, but also help solve the rough sea problem. All of the deghosting schemes (Robertsson and Kragh, 2002; Amundsen *et al.*, 1995) that try to deal with the rough sea problem in the frequency domain are limited since the sea surface is changing all the time. Deghosting in time domain seems a better approach.

3. NUMERICAL TESTS

In this chapter, I apply the Green's theorem deghosting method to both towed streamer and ocean bottom synthetic data. In Section 3.1, I present reasons why the Cagniard-de Hoop method is chosen to generate the data I used. Then in Section 3.2, numerical tests on towed streamer data are given. I first apply the deghosting algorithm to point receiver data. Then the deghosted data is put into the ISS free surface multiple removal (FSMR) algorithm. Since receiver arrays are widely used in practice, deghosting and ISS FSMR algorithms using receiver array data are tested in Section 3.3. Then, in Section 3.4, deghosting results are shown for the case when there is a small error in the depth of the receivers. Numerical tests of the deghosting algorithm applied to ocean bottom data are shown in Section 3.5

3.1 Data generation

As mentioned in Chapter 1, deghosting is one of the pre-requisites for the ISS free surface multiple removal, internal multiple removal, imaging without the velocity and non-linear inversion methods. A common feature of these ISS related algorithms is that the amplitude information as well as the arrival time of the data has been exploited. This is different from many other seismic processing procedures. The feedback free surface multiple attenuation method, for example, aims to predict the correct arrival time of the free surface multiples. Amplitude and shape of the predicted free surface multiples is less important, since adaptive subtraction is used to compensate the shape and amplitude difference between the predicted

free surface multiples and the real ones in the data.

Since those ISS related algorithms put a very high bar on the data processing, we need to deal with the amplitude as well as the arrival time of the data very carefully during deghosting. The first step is to generate high quality data. High quality data would also be helpful to locate problems if the deghosting results are not as good as expected.

The finite difference methods are good choices to generate high quality data. However, to better QC (quality control) the deghosting results, the Cagniard-de Hoop method (de Hoop and van der Hijden, 1983; Aki and Richards, 2002) is a much better choice. As mentioned in Chapter 2, the whole deghosting algorithm is performed in two steps: first deghosting on receiver side then deghosting on source side. When the deghosting on receiver side is finished, I would like to check the quality of the results. That means I need to know the exact receiver side deghosted results. But the finite difference method can not provide this receiver side deghosted data. It provides *all* of the data received at each receiver. The Cagniard-de Hoop method can generate very high quality of data and at the same time, I can *choose* to generate each event I am interested in. For example, I can easily generate the data that does not contain receiver ghosts but contain source ghosts.

For the model in Fig. 3.1, the wavefield at $(400m, 9m)$ and $(1400m, 9m)$ are shown in Fig. 3.2. Note that: (1) the arrival time of each event from the earliest to the latest is primary, source ghost, receiver ghost and source-receiver ghost; and (2) before and after deghosting, the amplitude and shape of the data are very different, while the arrival time is almost the same. The second point again stresses the value of deghosting is not just to predict the correct arrival time, but to predict the correct amplitude and shape. The Ricker source wavelet used to generate the data in Fig. 3.2 is shown in Fig. 3.3

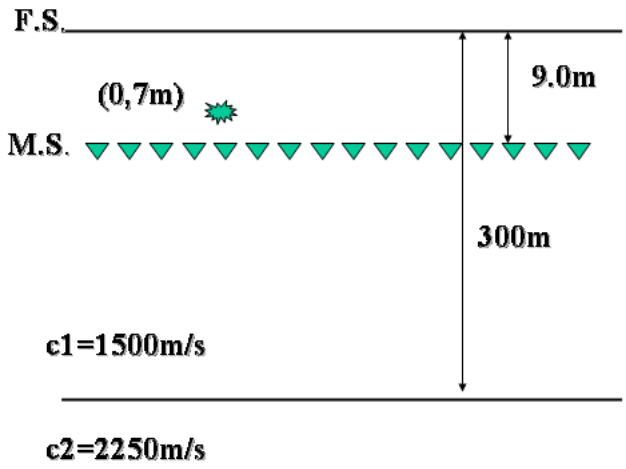

Fig. 3.1: *A simple acoustic model where constant density has been used. Wave velocity in water is 1500m/s.*

3.2 Deghosting and free surface multiple removal on towed streamer point receiver data

In this section, I present the numerical tests on towed streamer data measured by point receivers. Fig. 3.4 is the model I used. It is a constant density acoustic model with only one subsurface reflector. The wave velocity in the water is $1500m/s$.

I generated the towed streamer data using the Cagniard-de Hoop method. The source wavelet is the Ricker wavelet in Fig. 3.3. Using the generated data, I first perform field prediction at depth $4.0m$, then perform receiver side deghosting at depth $2.5m$. After that, I go to the common receiver gather and switch source and receiver position, then predict the field at depth $1.5m$. Finally, I perform source side deghosting at depth $1.0m$. So at last, I obtain the total source and receiver side deghosted field at depth $2.5m$ for a source at depth $1.0m$. The results are shown in Fig. 3.6 and compared with the exact deghosted field which is calculated using Cagniard-de Hoop method separately. Notice that using point receiver

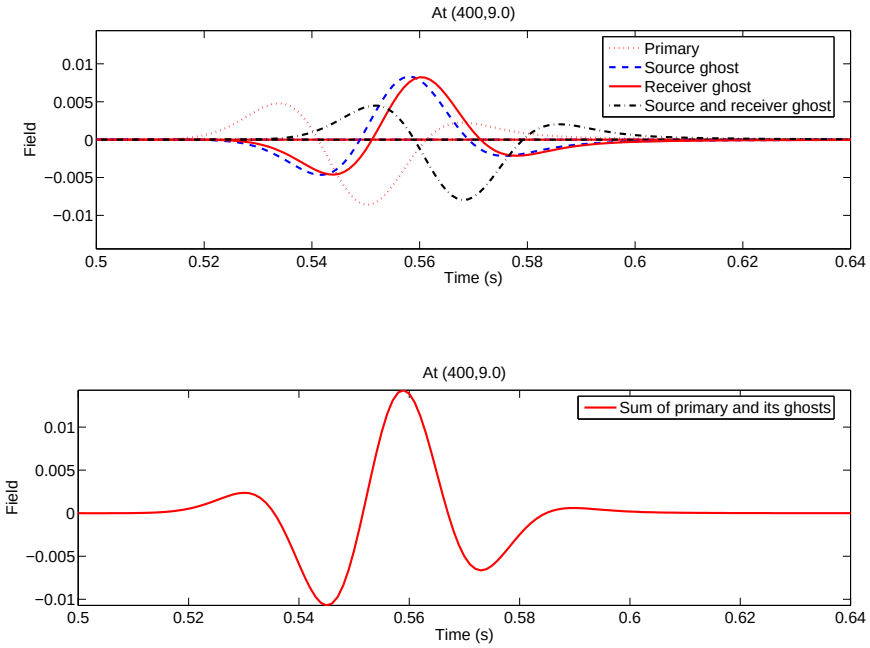

(a) Each events at (400,9)

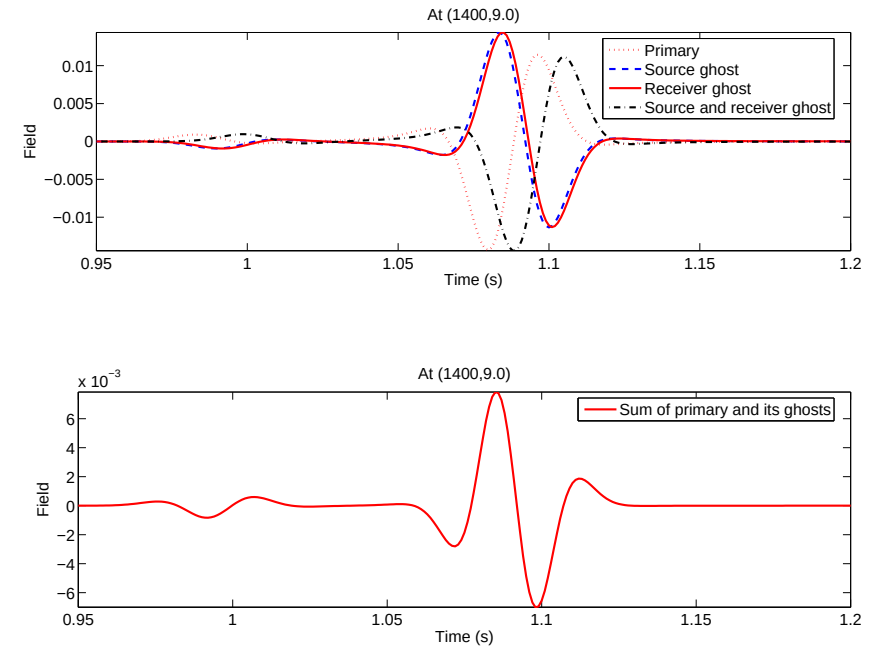

(b) Each events at (1400,9)

Fig. 3.2: *Data generated using Cagniard-de Hoop method. Sum of primary and its ghosts is the data before deghosting while primary is the data after deghosting*

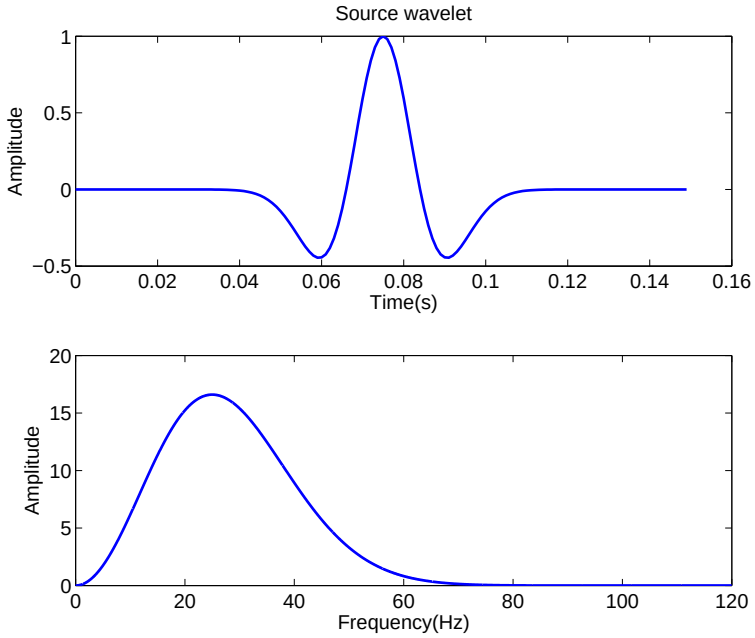

Fig. 3.3: *Ricker wavelet with dominant frequency 25Hz.*

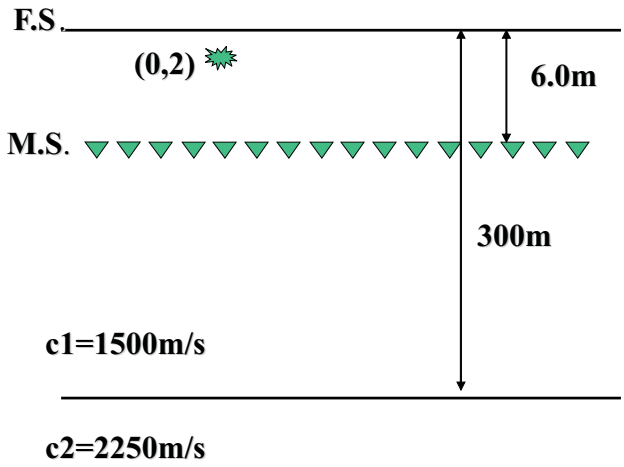

Fig. 3.4: *The constant density acoustic model for testing of deghosting and free surface multiple removal.*

data and the known source wavelet, very accurate deghosting results have been obtained. There is no visible difference between the exact result and the calculated deghosting result. Also, the direct wave which is very strong especially at zero offset in Fig. 3.5 has been eliminated in Fig. 3.6.

ISS free surface multiple removal is then applied to the deghosted data. The data before and after the FSMR are compared with each other in Fig. 3.7. The primaries are kept intact after FSMR and the first order free surface multiples have been eliminated. Since only the first term of the ISS FSMR series has been used, higher orders (> 1) of free surface multiples have been altered, instead of being eliminated. From Fig. 3.7, I can see that the second order free surface multiple has been kept exactly the same amplitude but the polarity has been changed. The amplitude of the third order free surface multiple is two time stronger after removal and the polarity has been changed too. All of the phenomena above are exactly expected according to the ISS FSMR algorithm. The higher order free surface multiples are altered so that they can be removed by other terms in the FSMR series. The first order free surface multiples were eliminated by a simple subtraction since they are predicted exactly by ISS FSMR algorithm. As mentioned in Chapter 2, this is the major difference between ISS FSMR algorithm and the feedback loop method, since the latter can only predict multiples at the roughly correct arrival time but the shape and amplitude are incorrect which means they can be removed only through adaptive subtraction. The ISS FSMR method has the capability of predicting the multiples accurately since it includes the obliquity factor (Carvalho, 1992; Weglein *et al.*, 1997) and requires source wavelet, source and receiver depth and deghosting. In practice, the exact prediction of free surface multiple is difficult due to receiver array effects (discussed in the next section), cable feathering (cable moving around while recording), rough sea surface and errors in estimation of source wavelet and deghosting. So adaptive subtraction is important in real data. The point is that if I try to provide as much requirements as possible then I can reduce the burden of

adaptive subtraction in practice.

3.3 Deghosting and free surface multiple removal on towed streamer receiver array data

In practice, in order to improve the signal/noise ratio in the recorded data, receiver arrays are widely used. Receiver array is an array of receivers whose records are summed together to produce one output. During the summation, the random noise hopefully can be mitigated while the signals become stronger. At the same time, the reference wave is mitigated by the receiver array also. One consequence of this summation process is that the output record does not satisfy the wave equation any more, which could cause problem for all of the wave equation derived algorithms such as deghosting and ISS FSMR.

In this section, I test the deghosting and ISS FSMR algorithm using receiver array data. The receiver array model I used is called Guardian (Fig. 3.8). Wavefields recorded by eight receivers are summed up to provide one output. The data generated using this receiver arrays are presented in Fig. 3.5. Notice that the receiver array data agree well with the point receiver data except small amplitude errors.

The deghosting result using the receiver array data is presented in Fig. 3.9. The direct wave has very strong residues. This strong residual direct wave will severely affect the performance of the ISS FSMR algorithm. In order to focus our attention on the most important scattered field, I re-calculated the receiver array data which does not contain the direct wave and perform deghosting again. The results are shown in Fig. 3.10. The zoom in version of Fig. 3.10 is shown in Fig. 3.11. So using receiver array data, the deghosting results are still very encouraging, although there is small errors (around 10%) in the amplitude of each event. The deghosted data are then put into the ISS FSMR algorithm. The data after FSMR is compared with data before FSMR in Fig. 3.12. Notice

that using receiver array data, the first order free surface multiple has been greatly damped instead of being eliminated. Also, the amplitude of higher order free surface multiples has not been altered exactly in the way they are supposed to be. Although the results are not as good as the case using point receiver data, they are still very encouraging since no adaptive subtraction was used.

3.4 Deghosting of towed streamer point receiver data: wrong depth

In this section, deghosting results are shown for the case of point receiver data containing a small depth error in the cable depth. The actual cable depth is $6.0m$ while the wrong depth of $6.6m$ is input. The deghosting result is shown in Fig. 3.13. Exact deghosting results at both $2.5m$ and $3.1m$ are shown. There is some residue of direct wave at zero offset. In Fig. 3.14 which is the zoom in version of Fig. 3.13. The result is still very good although there is a small amplitude error. I include the exact deghosting results at $3.1m$ because it is $4.5m$ above the wrong cable depth $6.6m$, just like $2.5m$ is $4.5m$ above the correct depth $6.0m$.

3.5 Deghosting of ocean bottom data

In this section, the deghosting algorithm is applied to ocean bottom data. On ocean bottom, both pressure and its vertical derivative are measured by hydrophone and geophone respectively at the same time. So in principle I can directly perform deghosting. However, there are several reasons not to directly use both measurements. The first reason is the different instrument response factor. On ocean bottom, the pressure/wavefield and its vertical derivative are measured by hydrophone and geophone respectively. Usually the instrument response factors of the two kinds of equipment are different. To achieve better processing results, it is necessary to calibrate the two response factors which is not an easy

task (Dragoset and Barr, 1994). The second reason is that the vertical derivative of the measurements can be inaccurate due to the loose attachment of the geophone to the ocean bottom. The last reason is that geophone measurements are usually very noisy.

As mentioned in Section 2.1.1, source wavelet, pressure measurement and its vertical derivative form a triangle relationship. Any one of the three can be calculated using the other two. Hence, I can *calculate* the vertical derivative of pressure as long as source wavelet and pressure measurements are available. The advantage of this method is that it can avoid the use of the noisy vertical derivative measurement. Most importantly, if one can assume the source wavelet is obtained through using the measurements of hydrophones in the towed streamers (which is often true due to the high cost of data acquisition on ocean bottom, ocean bottom data is usually measured after the towed streamer data has been processed), then the calculated vertical derivative of pressure will have exactly the same hydrophone instrument response factor and the effect of response factor on deghosting will be minimized.

The triangle relationship expressed in the frequency-wavenumber domain is

$$\frac{dP(k_x, z', x_s, z_s, \omega)}{dz} = \frac{A(\omega)e^{ik_x x_s}(e^{-ik_z z_s} - e^{ik_z z_s})}{e^{-ik_z z'} - e^{ik_z z'}} - ik_z P(k_x, z', x_s, z_s, \omega)\frac{e^{-ik_z z'} + e^{ik_z z'}}{e^{-ik_z z'} - e^{ik_z z'}}, \tag{3.1}$$

where z' is the depth of the ocean bottom, $k_z = \sqrt{k^2 - k_x^2}$ and $A(\omega)$ is the source wavelet. The advantages of using calculated $\frac{dP}{dz}$ instead of measured one have been listed above. The disadvantage of using Eq. 3.1 is the unstable spectral division. The actual $\frac{dP}{dz}$ is certainly always finite. So theoretically in the RHS of Eq. 3.1, when the denominator goes to zero, the numerator is supposed to approach zero (maybe at a different rate) in order to ensure the final result is finite. However, if there is noise or error in the numerator (P for example), the numerator might not approach zero or approach zero at a wrong rate, then the calculated $\frac{dP}{dz}$ will contain errors. For large cable depths, i.e., big z', the denominator can be zero

very often. In an attempt to solve this issue, in our numerical calculation, I only calculate the values of $\frac{dP(k_x,z',x_s,z_s,\omega)}{dz}$ at those k_x where the absolute value of the denominator is far from zero (e.g., > 0.3). Then the values of $\frac{dP(k_x,z',x_s,z_s,\omega)}{dz}$ at those unstable points will be interpolated using cubic spline interpolation (Press *et al.*, 1996) which guarantees the second derivative of the interpolated function is continuous. Fig. 3.15 illustrates this technique. As shown later in the deghosting results, there are still some artifacts.

Fig. 3.16 illustrates the primary, its ghosts, and their summation on the ocean bottom in Fig. 3.4. Apparently, the summation of these events is very different from the primary. Most importantly, the receiver ghost and the source-receiver ghost arrive significantly later than the primary and its source ghost at small offsets, due to the big depth of the receivers. Detailed explanation of each event is given in Fig. 3.17. The direct wave (Event (a)) arrives at exactly the same time as the primary (Event (b)). The only difference is that the former one does not hit the earth while the latter one hits the earth first then is recorded by the hydrophone. Similarly, the receiver ghost of the primary (Event (c)) arrives exactly at the same time as the first order free surface multiple (Event (d)) and the source-receiver ghost of the primary (Event (e)) arrives exactly at the same time as the source ghost of the first order free surface multiple (Event (f)).

If I simply convolve the ocean bottom data with itself to predict free surface multiples, the arrival time of the predicted first order free surface multiple can be *very* different from the actual one. So a separate data extrapolation operation to move the data from ocean bottom to the free surface is needed in order to ensure that the predicted free surface multiple has approximately the right arrival time. This step is performed naturally in the inverse scattering series based free surface multiple removal method.

Fig. 3.18 is the plot of the data before deghosting. It only includes the primary and its ghost events. Notice that at small offsets, the receiver ghost and source-receiver ghost arrive significantly late compared to the primary and its source ghost. As shown later, even for

this simple data set (which does not include the direct wave and its ghost, or any multiples or primaries), there are still a lot of artifacts. Fig. 3.19 presents the calculated and exact deghosting results. The calculated deghosting results is encouraging since the receiver ghost and source-receiver ghost have been removed. However, after bringing up the details of Fig. 3.19 (a), the artifacts in Fig. 3.20 are obvious. The artifacts are mainly due to the transform to the wavenumber domain and the spectral division.

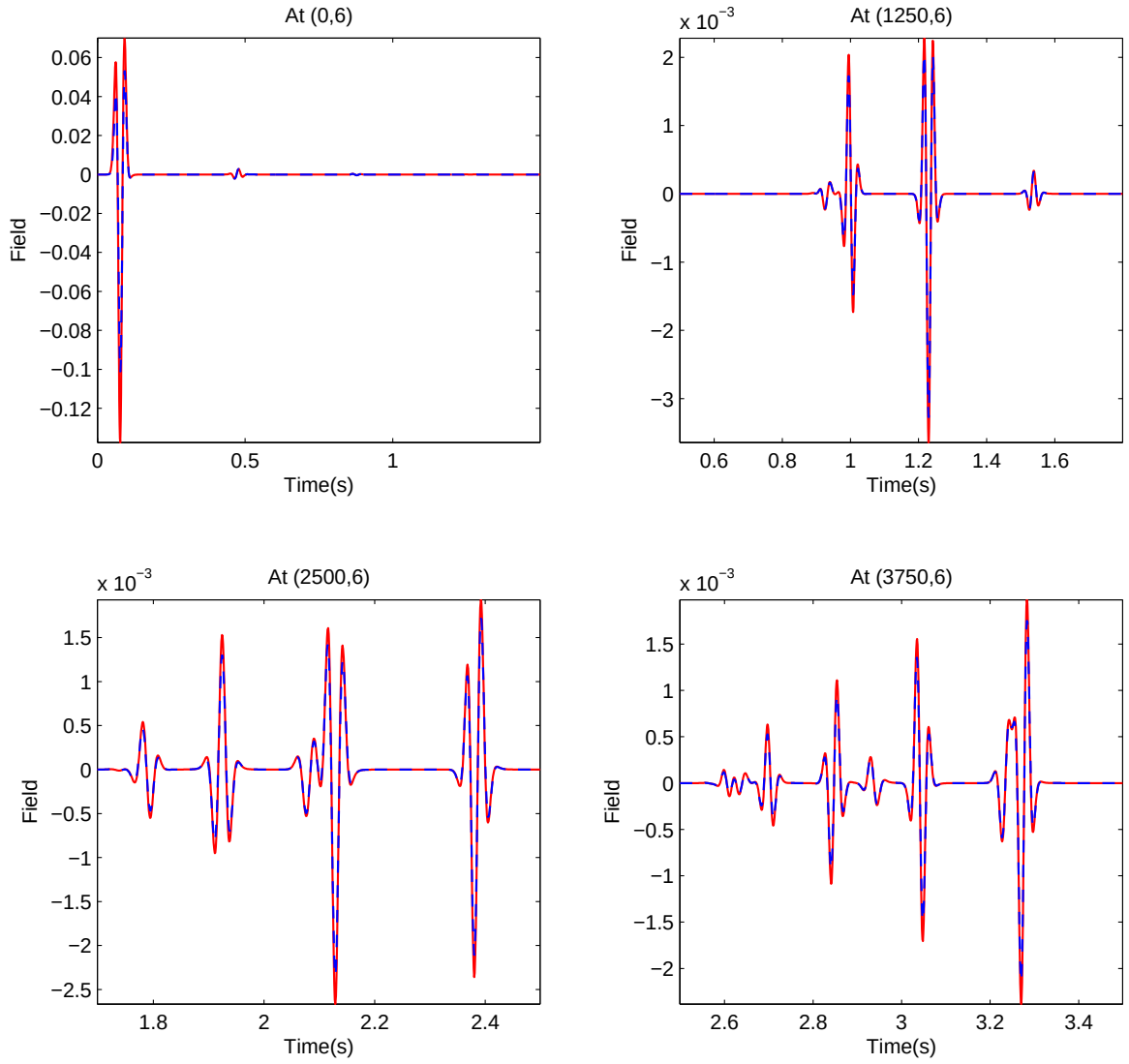

Fig. 3.5: *Tower streamer point receiver data (Red solid) and receiver array data (Blue dash) at four different offsets* $0m$, $1250m$, $2500m$ *and* $3750m$.

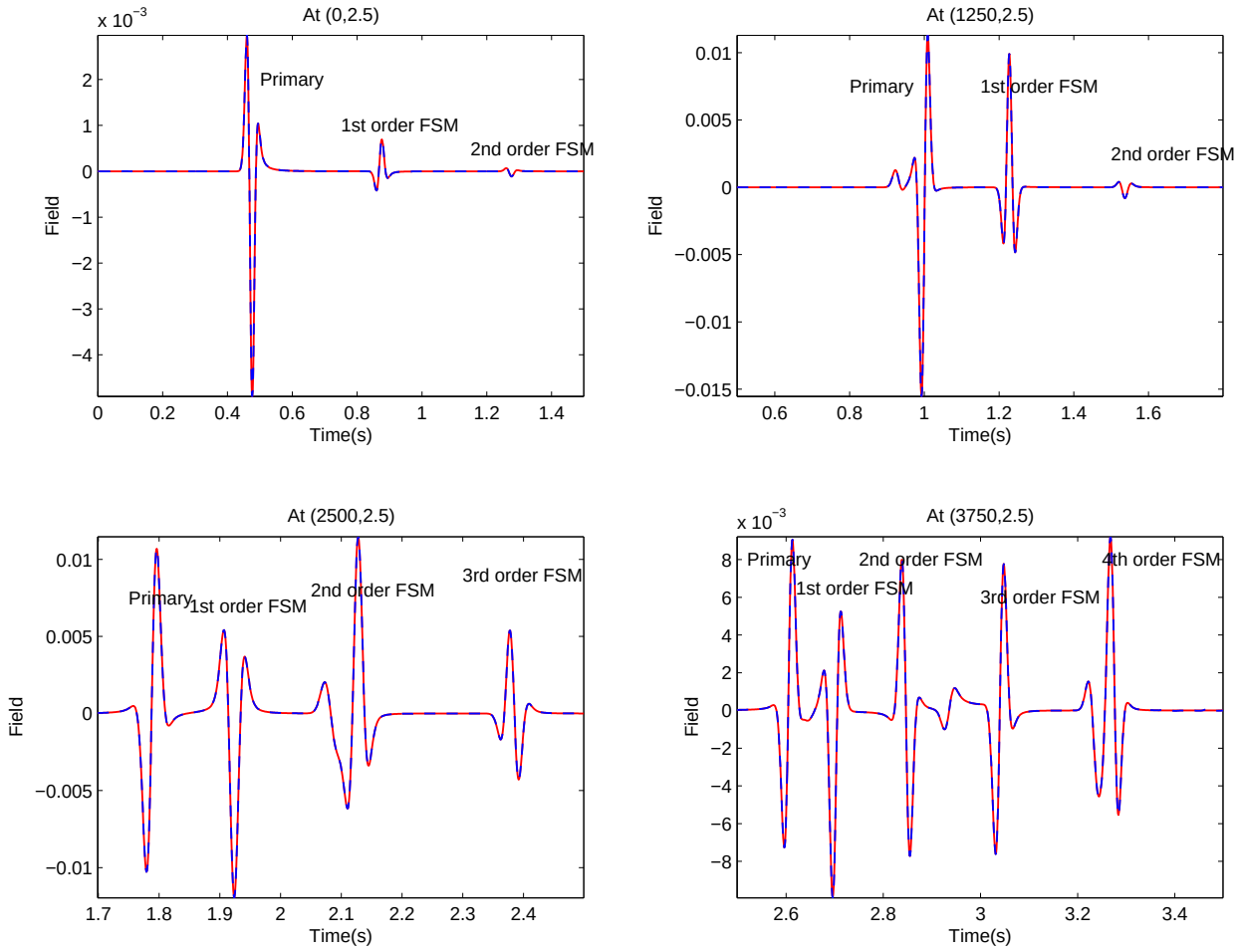

Fig. 3.6: *Using point receiver data, the calculated deghosting results (blue dash) are compared to the exact deghosting results (red solid). The two plots agree very well each other. There is no visible difference between the two results (Errors will change with respect to time and offset. But in the above listed offsets, the error of the peaks are less than 5%).*

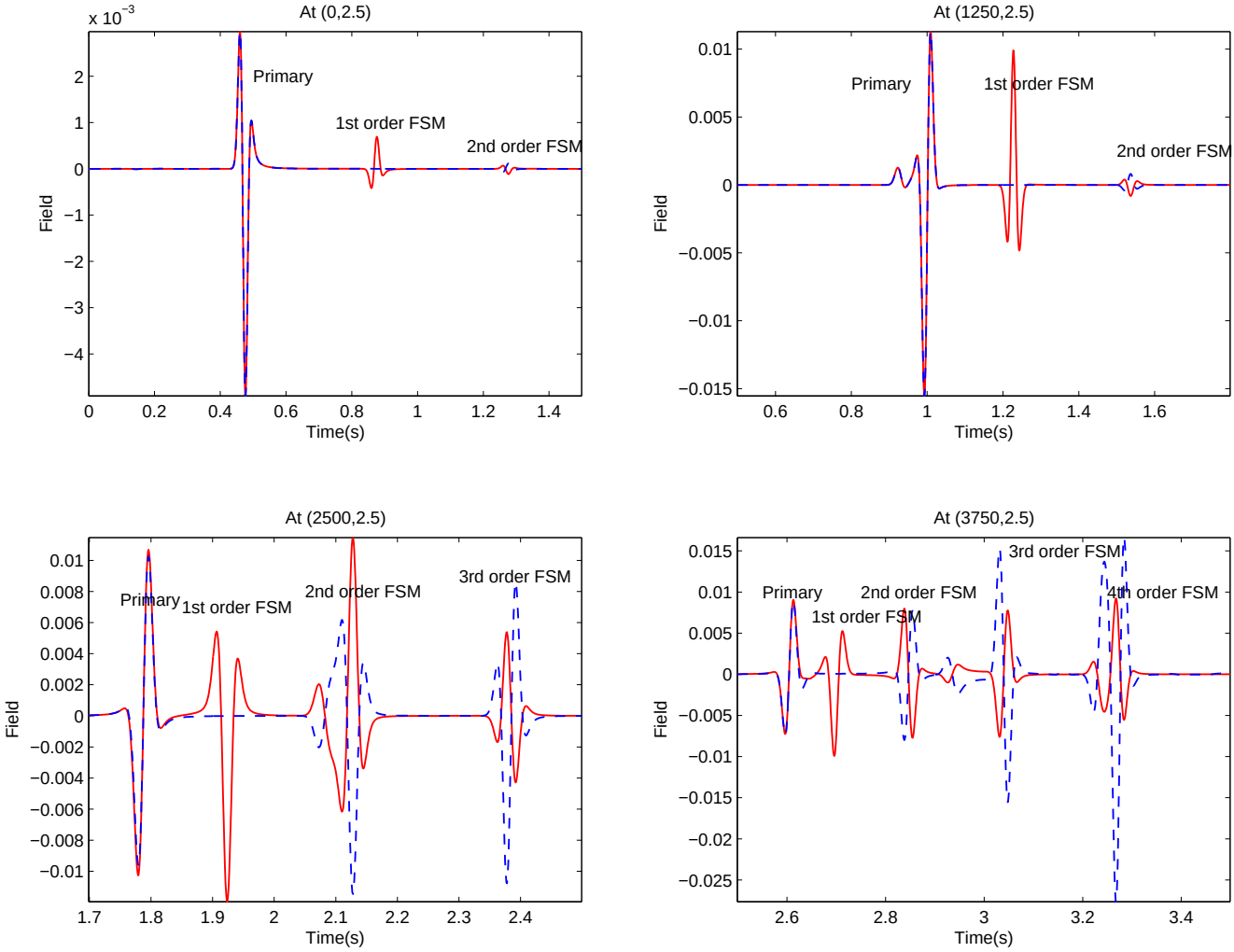

Fig. 3.7: *Using the first term in the ISS free surface multiple removal algorithm, the results after free surface multiple removal. Red solid: Data before free surface multiple removal. Blue dash: Data after free surface multiple removal. Primaries are kept intact and first order multiples have been eliminated though a simple subtraction. Higher order multiples are altered as expected so that they can be removed by higher order terms in the ISS FSMR series. Note that the data used for FSMR is source and receiver deghosted data.*

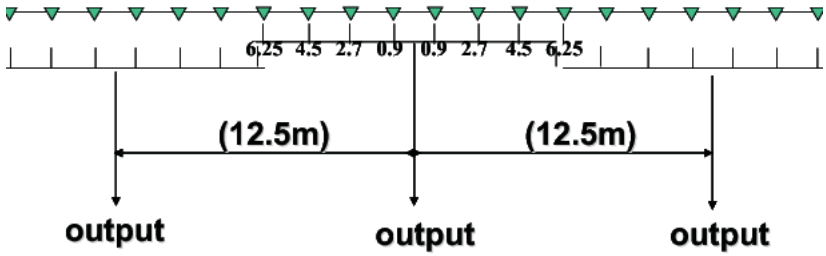

Fig. 3.8: Receiver array model (Guardian) used to receiver array data testing.

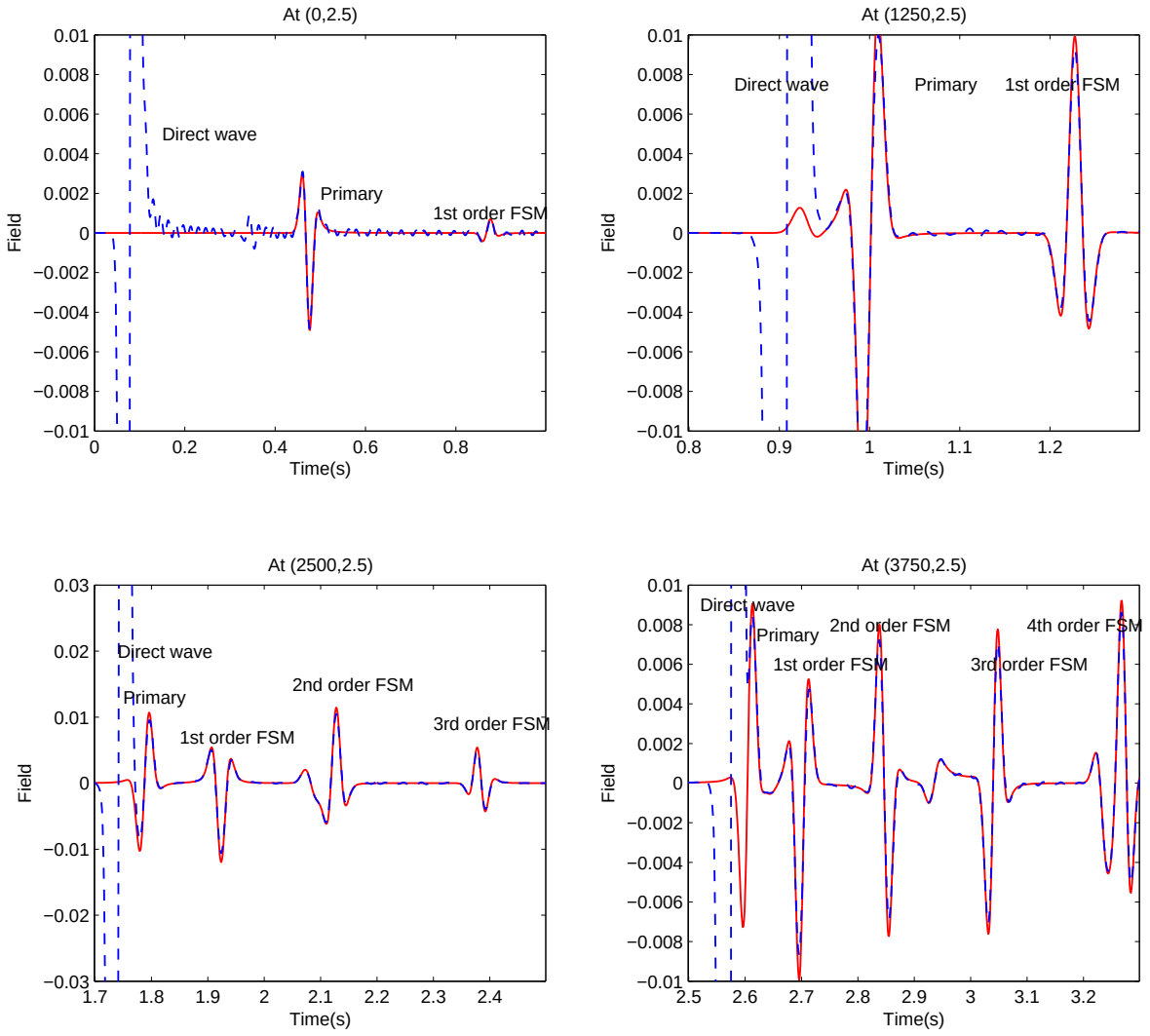

Fig. 3.9: *Using receiver array data, the calculated deghosting results (blue dash) are compared to the exact deghosting results (red solid). Notice the direct wave has not been removed.*

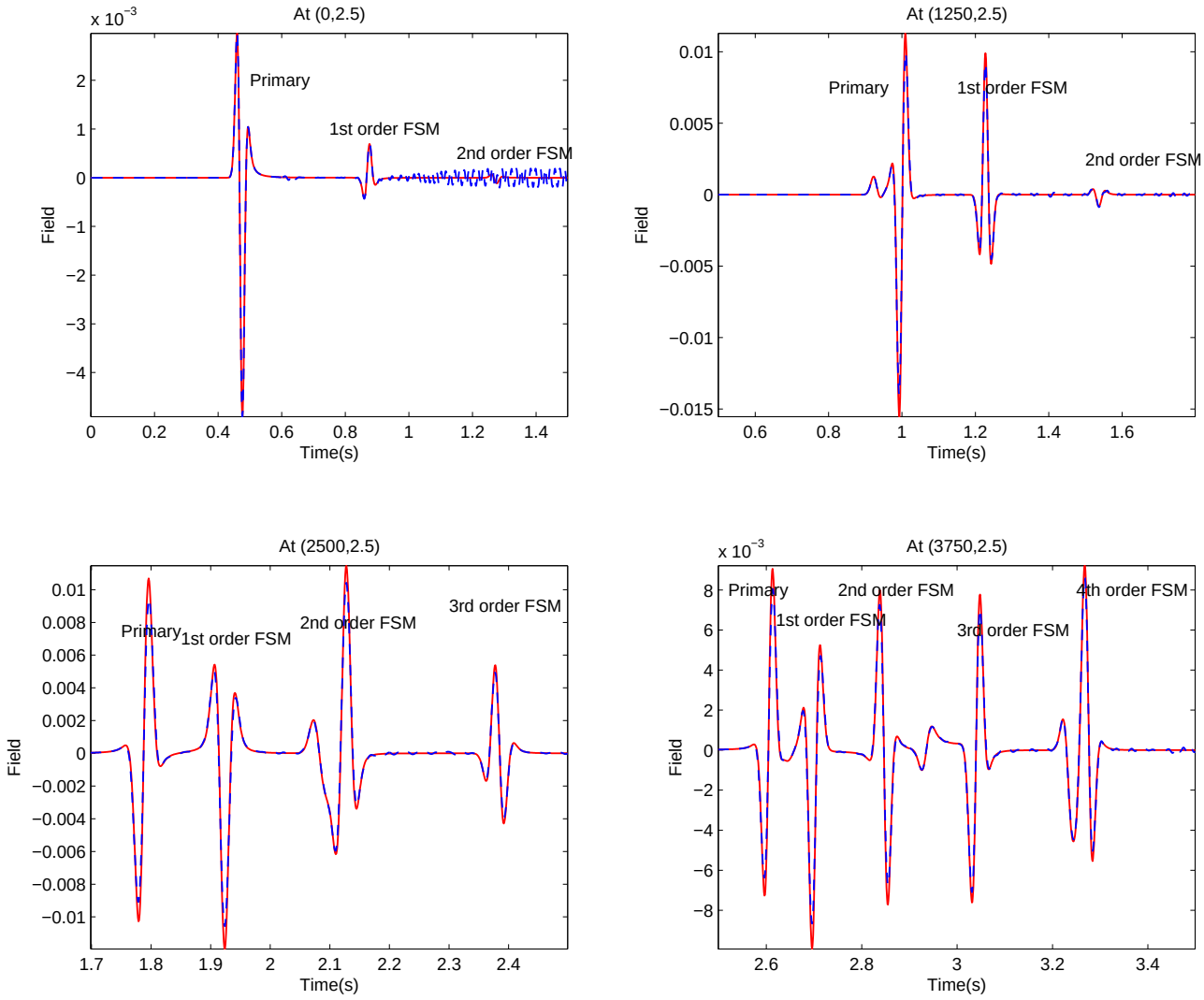

Fig. 3.10: *Using receiver array data, the calculated deghosting results (blue dash) are compared to the exact deghosting results (red solid). The direct wave has been removed before deghosting.*

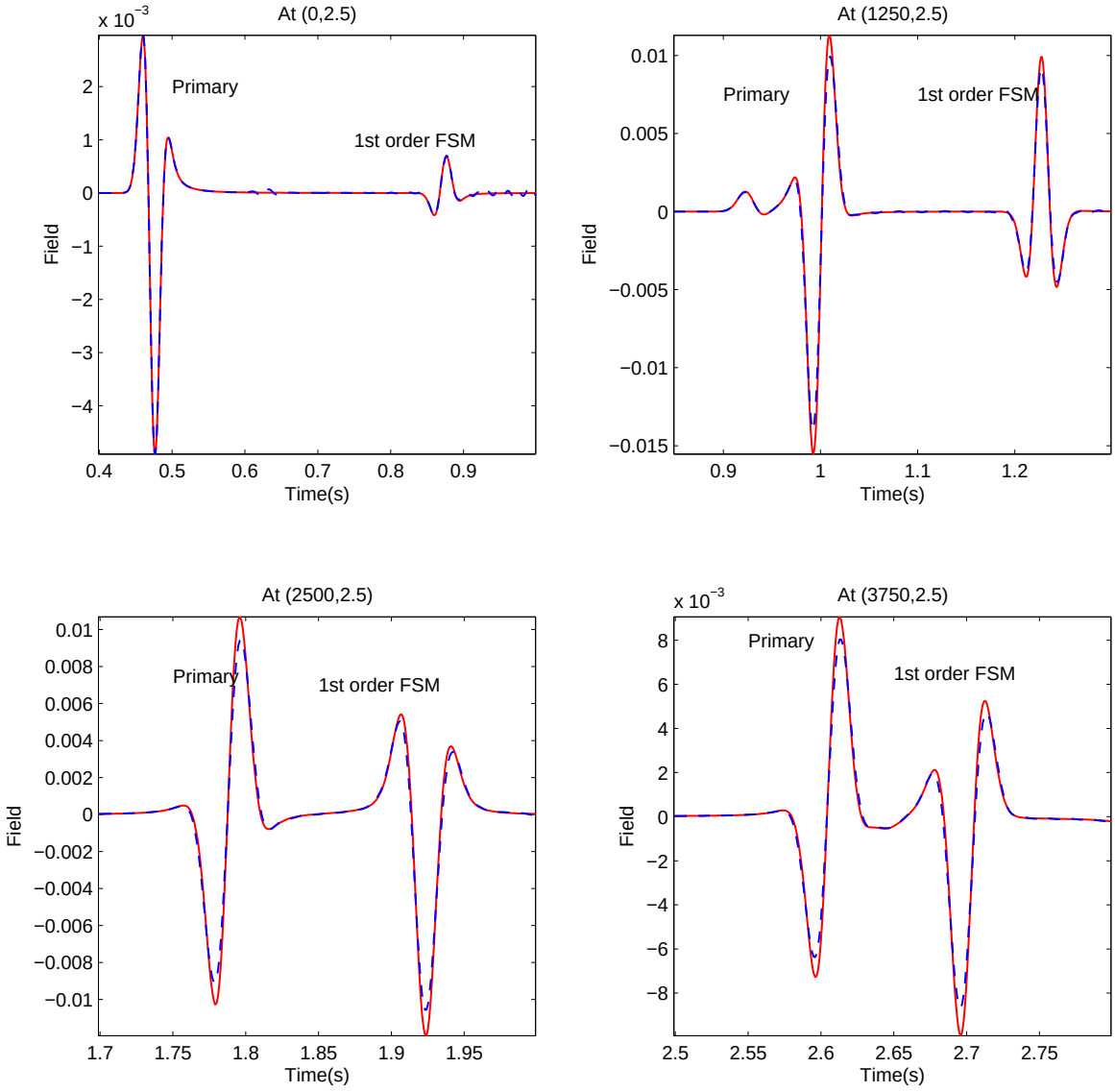

Fig. 3.11: *Enlarged version of Fig. 3.10 Using receiver array data, the calculated deghosting results (blue dash) are compared to the exact deghosting results (red solid). The direct wave has been removed before deghosting. Notice the small errors in amplitude.*

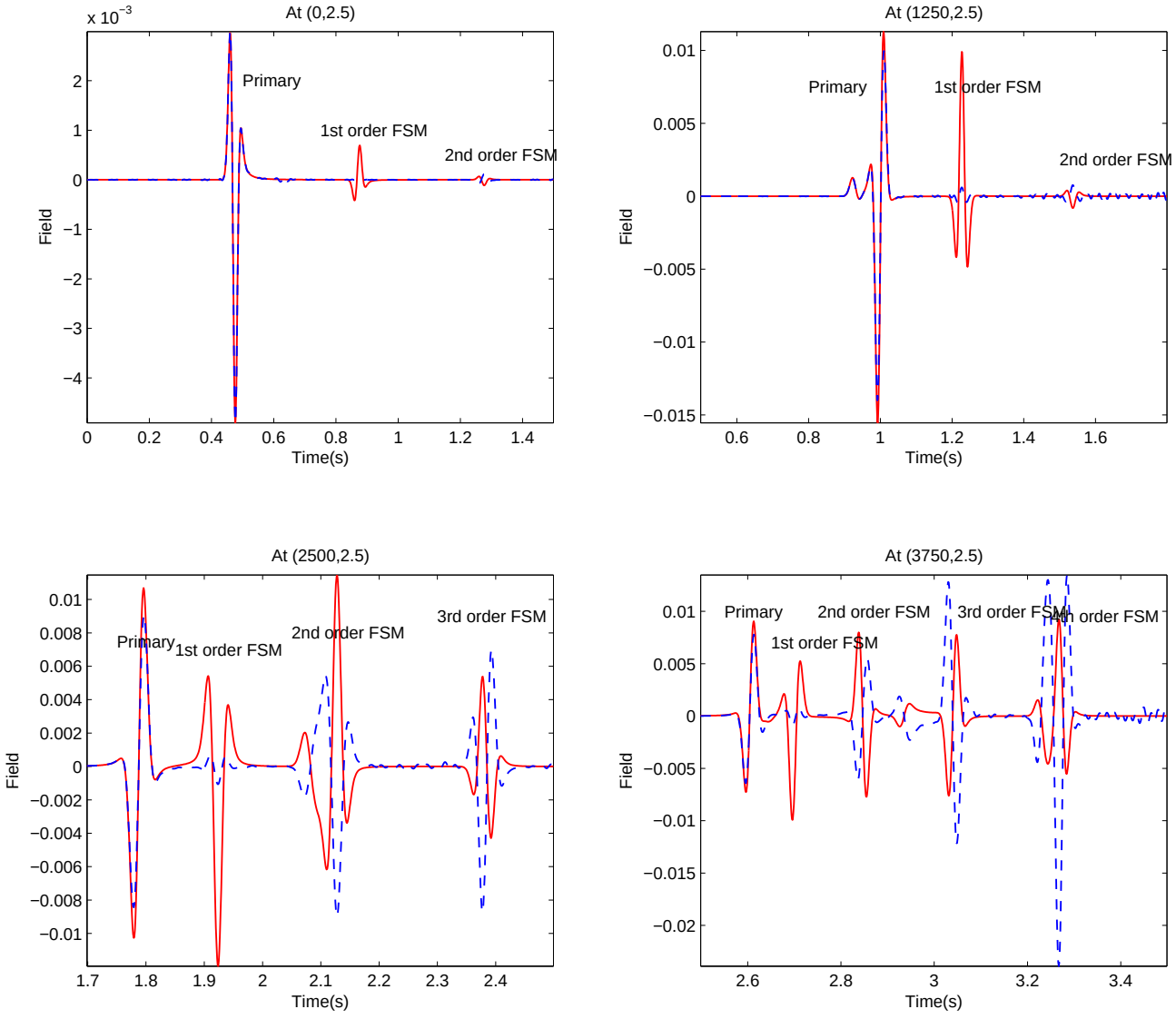

Fig. 3.12: *Using receiver array data, the results after free surface multiple removal (blue dash) are compared to the results before free surface multiple removal (red solid).*

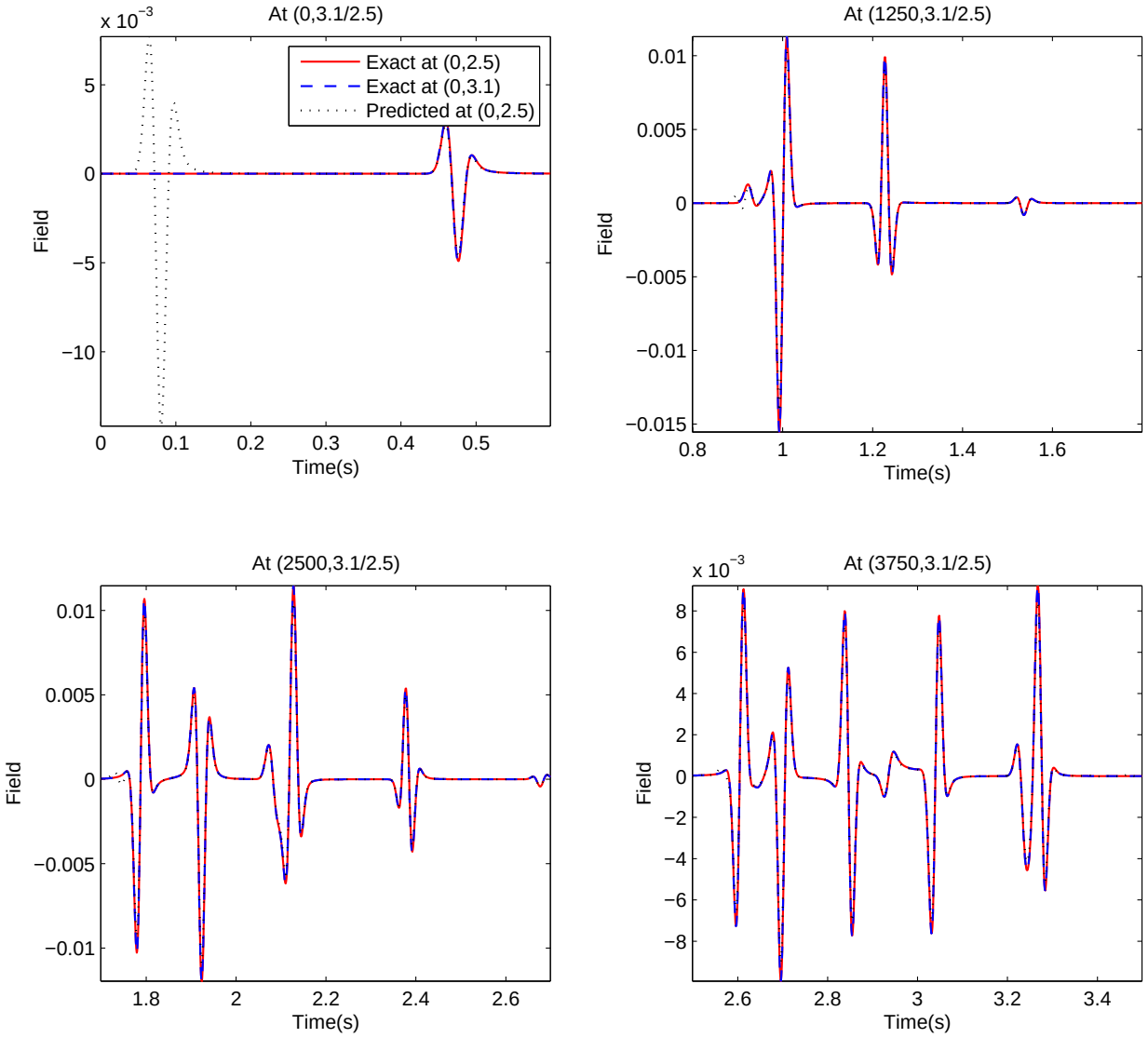

Fig. 3.13: *Using point receiver data, the deghosting results using incorrect receiver depth. The correct receiver depth is 6.0m while the used depth is 6.6m. The deghosting results are calculated at 2.5m. Exact deghosting results at 2.5m and 3.1m are also presented.*

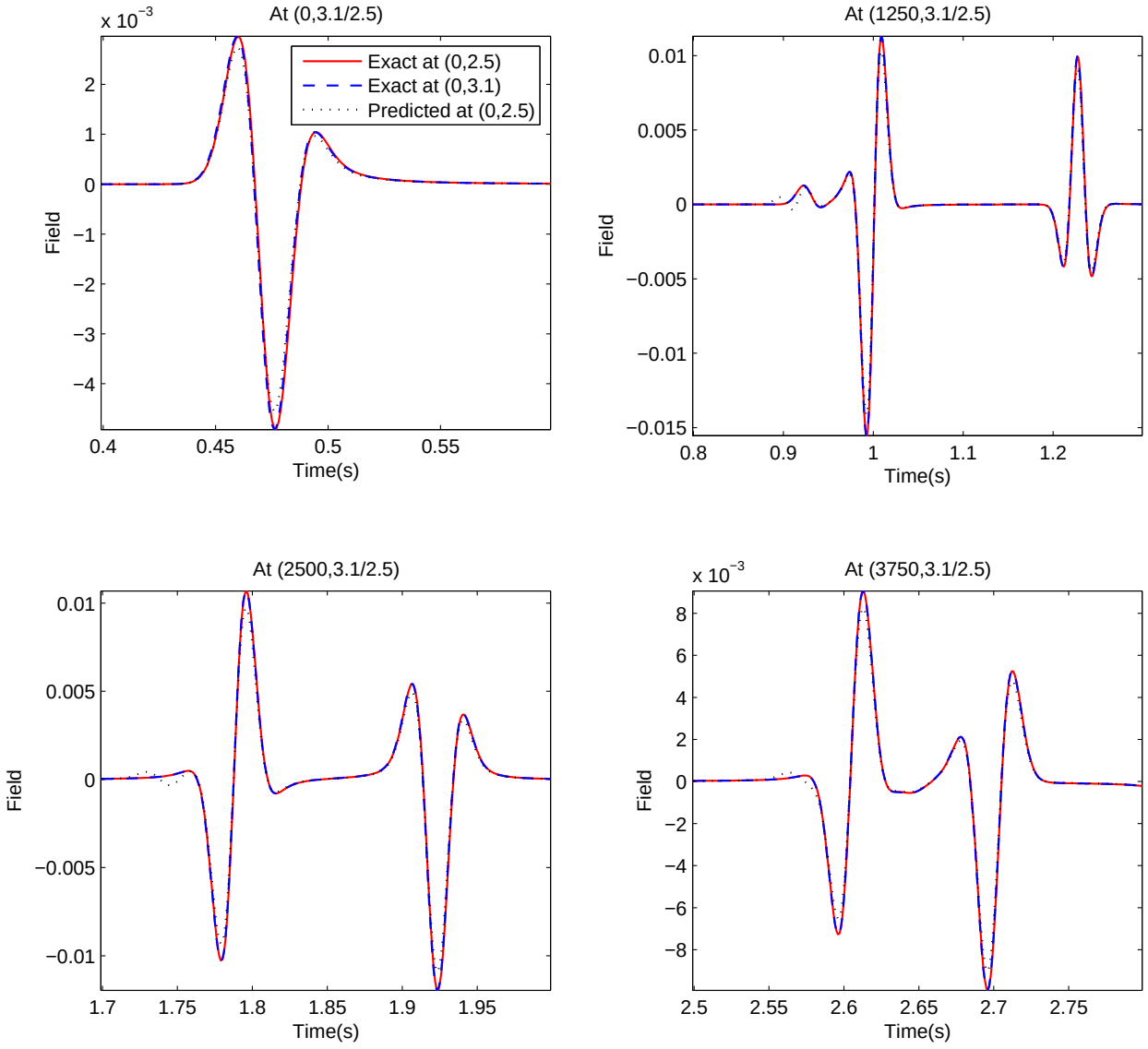

Fig. 3.14: *Using point receiver data, the deghosting results using incorrect receiver depth. The correct receiver depth is 6.0m while the used depth is 6.6m. The deghosting results are calculated at 2.5m. Exact deghosting results at 2.5m and 3.1m are also presented. This is the zoom in version of Fig. 3.13*

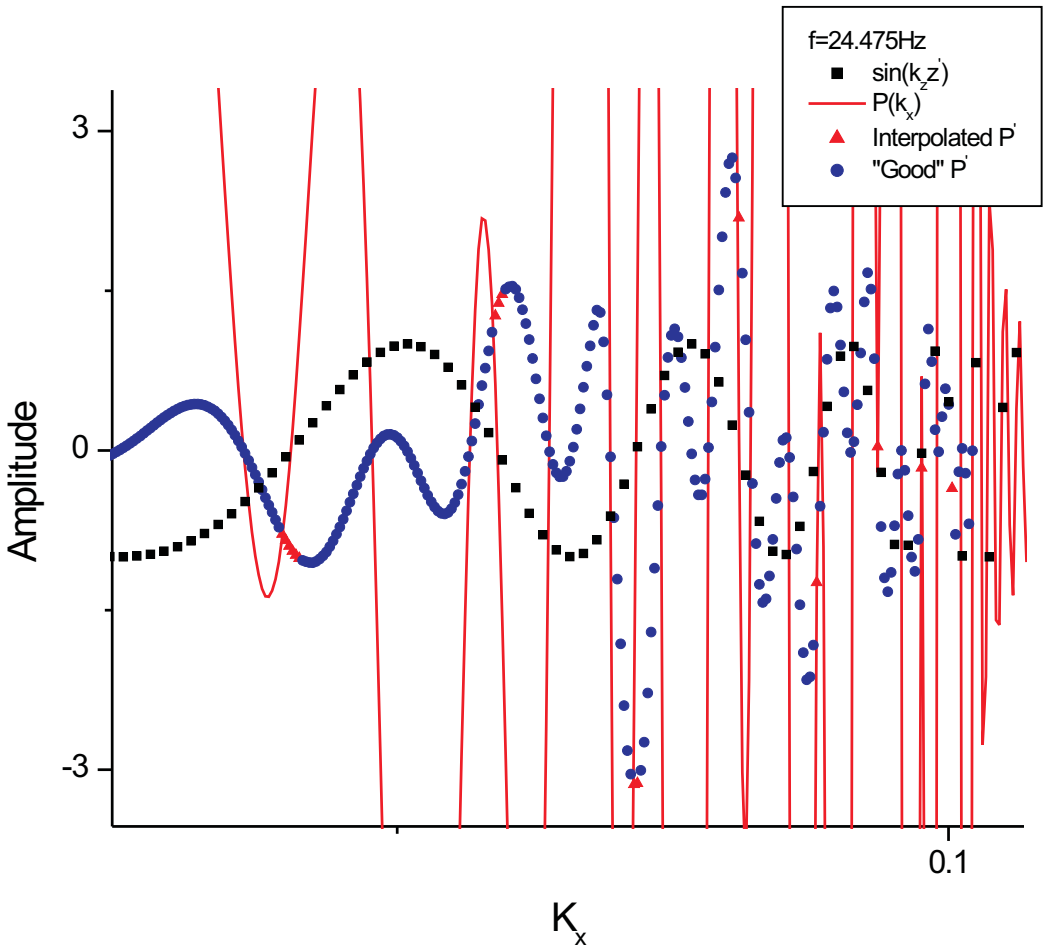

Fig. 3.15: *Demonstration of the interpolation schemes.* k_x *is the horizontal wavenumber with dimension* m^{-1}. *Square line:* $sin(k_z z')$; *Solid line:* $P(k_x)$; *Squares: Interpolated* P' *or* $\frac{dP}{dz}$; *Dots: Stable* $\frac{dP}{dz}$ *obtained by direct division instead of interpolation. When* $sin(k_z z')$ *approaches zero, those* $\frac{dP}{dz}$ *need to be interpolated.*

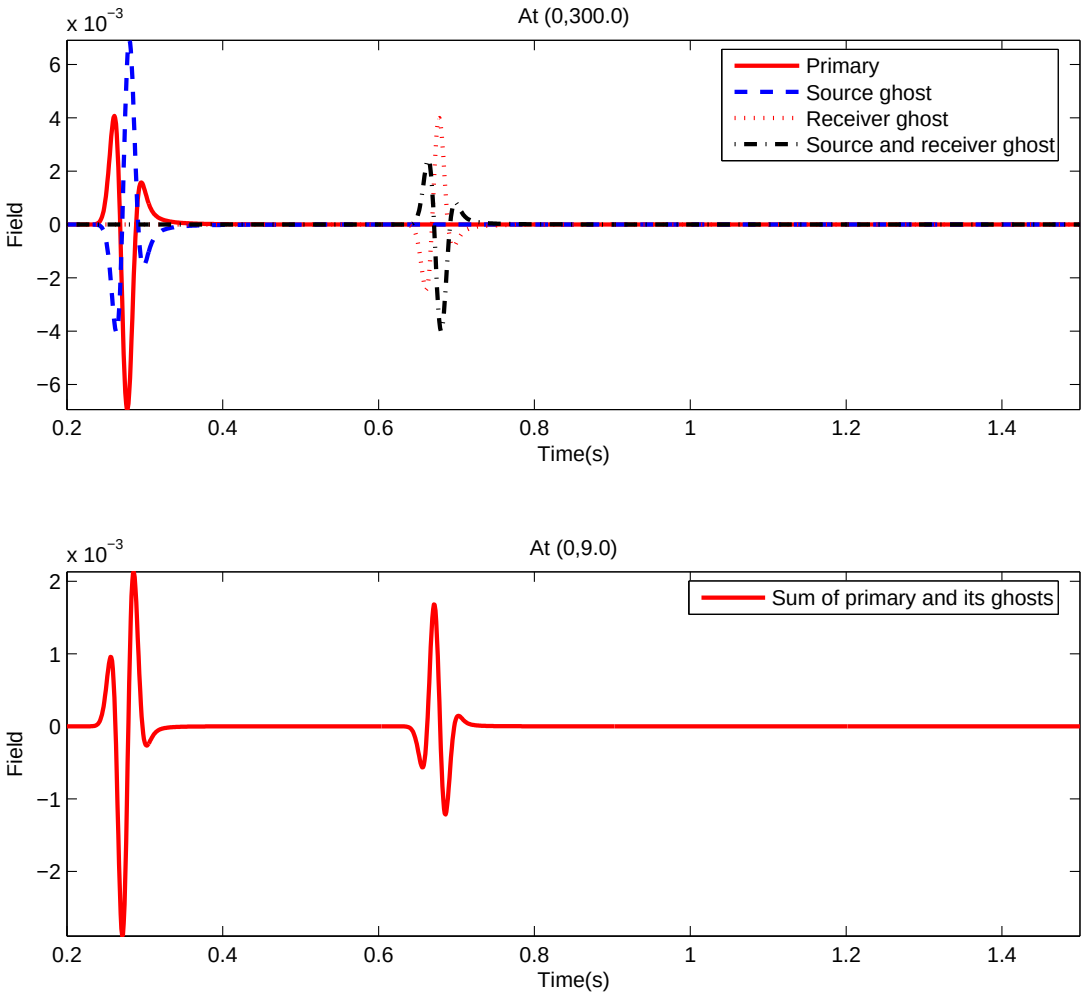

Fig. 3.16: *Ocean bottom primary and its ghost events.*

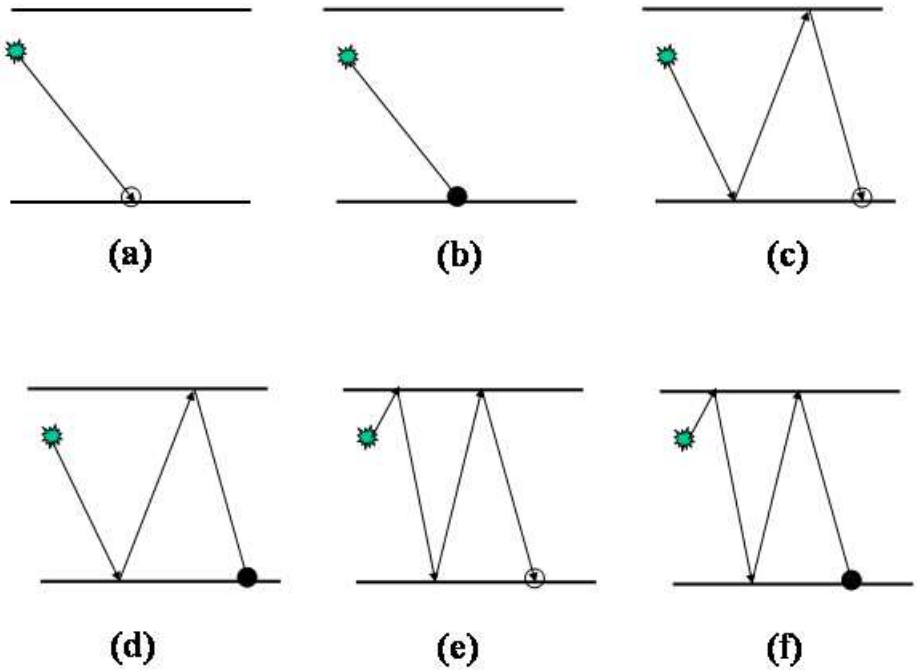

Fig. 3.17: *Empty circle means the wave does not hit the earth and solid circle means the wave hit the earth and then reflected upward and recorded by the receiver. (a): The direct wave; (b) The primary; (c) The receiver ghost of the primary; (d) The first order free surface multiple; (e) The source-receiver ghost of the primary and (f) The source ghost of the first order free surface multiple.*

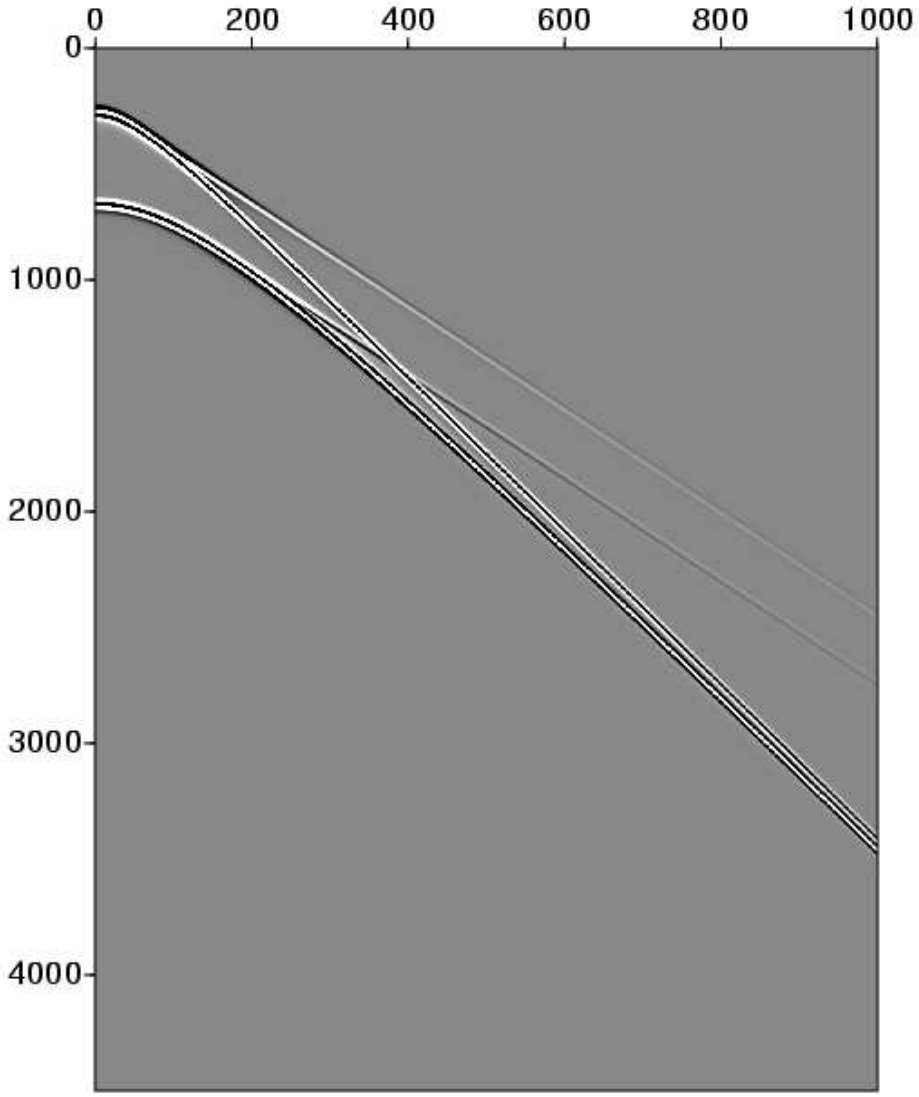

Fig. 3.18: *Ocean bottom data before deghosting. The horizontal axis is offset (m), and the vertical axis is time (ms).*

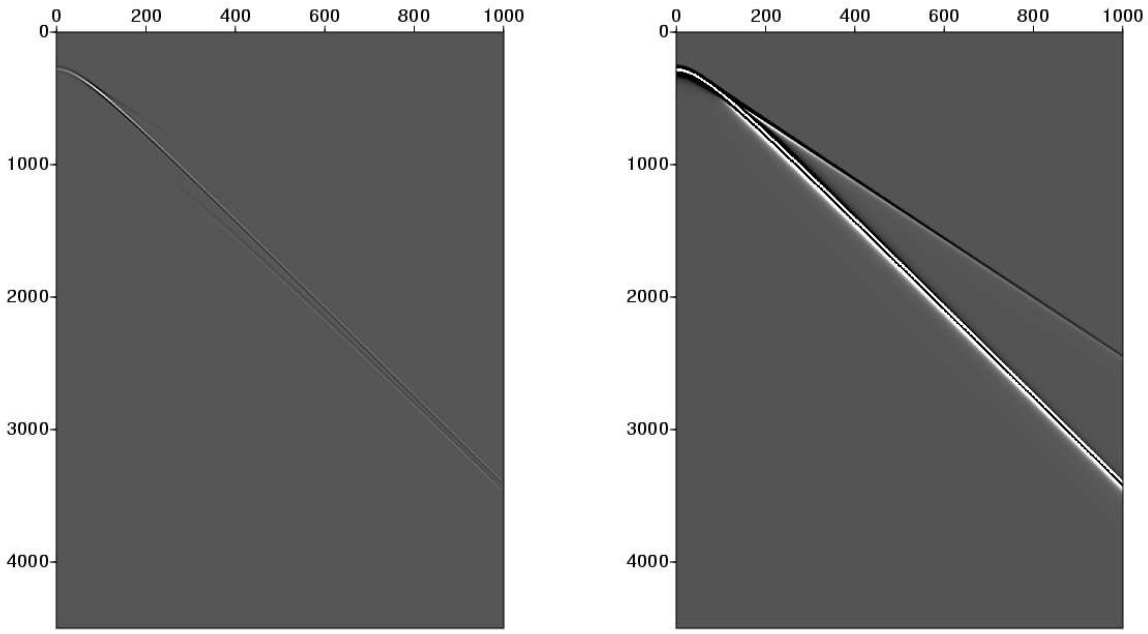

(a) Calculated deghosting result

(b) Exact deghosting result

Fig. 3.19: *Comparison of calculated and exact deghosting results. The horizontal axis is offset (m), and the vertical axis is time (ms).*

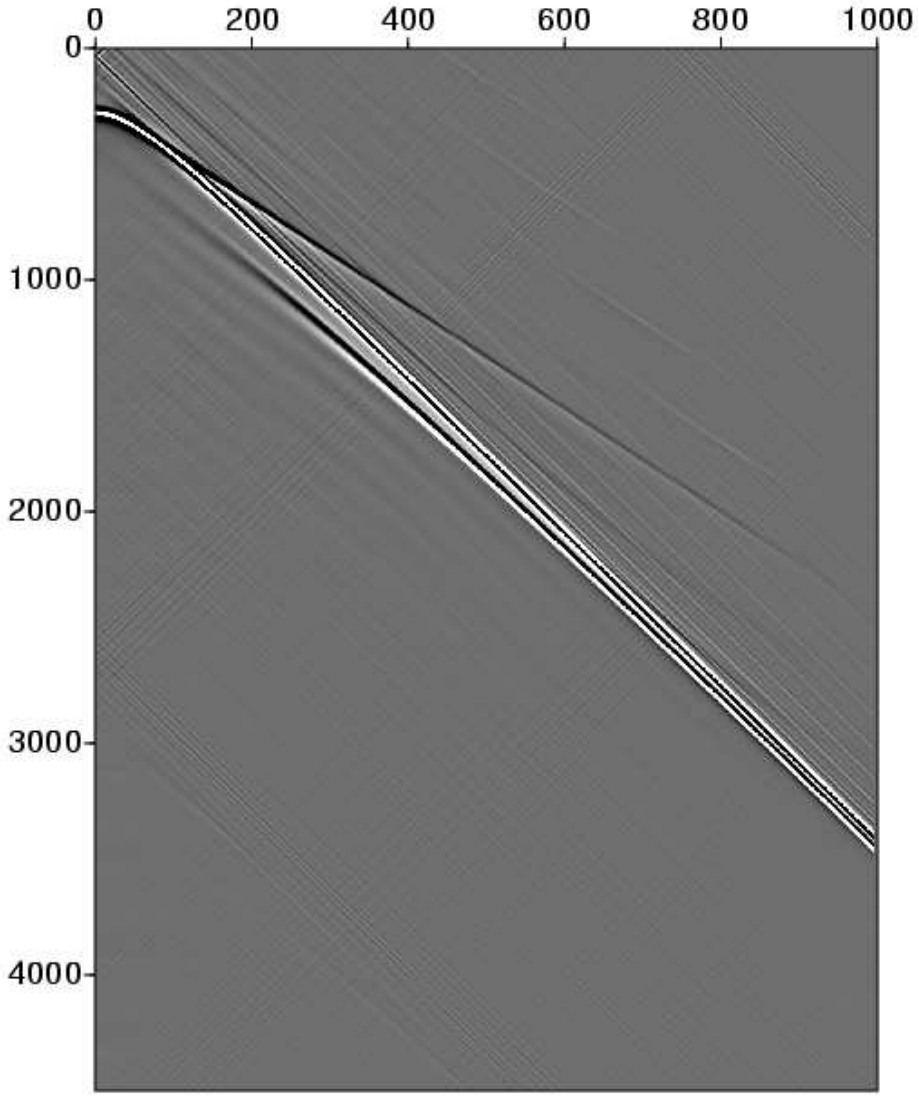

Fig. 3.20: *Zoom in version of Fig. 3.19 (a). The horizontal axis is offset (m), and the vertical axis is time (ms).*

4. SUMMARY

In this dissertation, I have developed, analyzed and tested a Green's theorem deghosting algorithm and its closely related wavelet estimation and wavefield prediction algorithms. When the assumptions of the deghosting algorithm are satisfied, very good deghosting results can be obtained. Those assumptions include the source wavelet, accurate cable depth and point receiver data on the measurement surface. For most of conventional towed streamer data, where only pressure measurements are available, I also assume that the free surface is flat and the wavefield on the free surface is zero. The deghosting result is put into inverse scattering series (ISS) free surface multiple removal (FSMR) algorithm and the first order free surface multiples are eliminated by a simple subtraction.

Very encouraging deghosting results can also be obtained when using receiver array data. The consequence of the small amplitude error in the deghosting results due to the use of receiver array data is that the ISS FSMR can greatly reduce the amplitude of the free surface multiples, instead of eliminating them (without using adaptive subtraction).

If there is a small depth error in the depth of the cable, the deghosting result can also produce encouraging results.

On ocean bottom data, assuming known source wavelet and using the triangle relationship among source wavelet, pressure and its vertical derivative, the vertical derivative of pressure is calculated so that I can avoid the use of troublesome geophone measurements. The issue of different instrument response factor between hydrophones and geophones can also be

avoided. In the calculation of the vertical derivative, spectral division can cause some artifacts. Further efforts are needed in order to mitigate or remove those artifacts.

New advances in receiver technology that measure both pressure and its vertical derivative provide opportunities for better performance of the deghosting, wavelet estimation and field prediction algorithms. I anticipate that generalization and extension of the methods developed and/or analyzed in this dissertation for source signature estimation and deghosting will be able to accommodate source arrays and rough sea.

REFERENCES

Abma, R., Kabir, N., Matson, K. H., Michell, S., Shaw, S. A., and McLain, B. 2005. Comparisons of adaptive subtraction methods for multiple attenuation. *The Leading Edge 24,* 3 (March), 277–280.

Aki, K. and Richards, P. G. 2002. *Quantitative seismology*, Second ed. University Science Books.

Amundsen, L., Rϕsten, T., Robertsson, J. O. A., and Kragh, E. 1995. Extraction of normal component of the particle velocity from marine pressure data. *Geophysics 60,* 1 (January-February), 212–222.

Amundsen, L., Secrest, B. G., and Arntsen, B. 2005. Rough-sea deghosting of streamer seismic data using pressure gradient approximations. *Geophysics 70,* 1 (January-February), V1–V9.

Araújo, F. V. 1994. Linear and non-linear methods derived from scattering theory: backscattered tomography and internal multiple attenuation. Ph.D. thesis, Universidade Federal da Bahia.

Born, M. and Wolf, E. 1999. *Principles of optics*, 7th ed. Cambridge University Press.

Carlson, D., Sollner, W., Tabti, H., Brox, E., and Widmaier, M. 2007. Increased resolution of seismic data from a dual sensor streamer cable. *SEG Expanded Abstracts. 26*, 994–998.

Carvalho, P. M. 1992. Free-surface multiple reflection elimination method based on nonlinear inversion of seismic data. Ph.D. thesis, Universidade Federal da Bahia.

de Hoop, A. T. and van der Hijden, J. H. M. T. 1983. Generation of acoustic waves by an impulsive line source in a fluid/solid configuration with a plane boundary. *J. Acoust. Soc. Am. 74*, 333–342.

Dragoset, W. and Barr, F. J. 1994. Ocean-bottom cable dual-sensor scaling. *SEG Expanded Abstracts*, 857–860.

Fokkema, J. T. and van den Berg, P. M. 1993. *Seismic Applications of Acoustic Reciprocity*, 1st ed. Elsevier Science.

Innanen, K. A. and Weglein, A. B. 2003. Simultaneous imaging and inversion with the inverse scattering series. In *Proceedings of the Eighth International Congress of the SBGf and Fifth Latin American Geophysical Conference*. SBGf.

Liu, F., Weglein, A., Innanen, K., and Nita, B. 2005. Extension of the non-linear depth imaging capability of the inverse scattering series to multidimensional media: strategies and numerical results. In *SBGf (Sociedade Brasileira de Geofísica) Expanded Abstracts*. SBGf.

Matson, K. H. and Abma, R. 2005. Fast 3d surface-related multiple elimination using azimuth moveout for multiples. *SEG Expanded Abstracts. 24*, 2064–2067.

Matson, K. H. and Zhang, J. 2007. Improving the accuracy of 'fast' 3d SRME. *SEG Expanded Abstracts. 26*, 2481–2483.

Moldoveanu, N., Combee, L., Hampson, G., Sydora, L., and Abriel, W. 2007. Over/under towed-streamer acquisition: A method to extend seismic bandwidth to both higher and lower frequencies. *The Leading Edge 26*, 41–58.

Osen, A., Secrest, B. G., and Amundsen, L. 1998. Wavelet estimation from marine pressure measurements. *Geophysics 63,* 6 (November-December), 2108–2119.

Press, W. H., Teukolsky, S. A., Vetterling, W. T., and Flannery, B. P. 1996. *Numerical Recipes in Fortran 90*, Second ed. Cambridge University Press.

Ramírez, A. 2007. I. Inverse scattering sub-series for removal of internal multiples and depth imaging primaries, and II. green's theorem as the foundation of interferometry and guiding new practical methods and applications. Ph.D. thesis, University of Houston.

Ramírez, A. C. and Weglein, A. 2005. An inverse scattering internal multiple elimination method: Beyond attenuation, a new algorithm and initial tests. *SEG Expanded Abstracts.*, 2115–2118.

Robertsson, J. and Kragh, E. 2002. Rough sea deghosting using a single streamer and a pressure gradient approximation. *Geophysics 67*, 2005–2011.

Schneider, W. A., Larner, K. L., Burg, J. P., and Backus, M. M. 1964. A new data processing technique for the elimination of ghost arrivals on reflection seismograms. *Geophysics 29*, 783–805.

Shaw, S. A., Weglein, A. B., Matson, K. H., and Foster, D. J. 2002. Cooperation of the leading order terms in an inverse-scattering subseries for imaging: 1-d analysis and evaluation. *SEG Technical Program Expanded Abstracts*, 2277–2280.

Tan, T. 1999. Wavelet spectrum estimation. *Geophysics 64,* 6 (November-December), 1836–1846.

Verschuur, D. J., Berkhout, A. J., and Wapenaar, C. P. A. 1992. Adaptive surface-related multiple elimination. *Geophysics 57*, 1166–1177.

Weglein, A. B., Araújo, F. V., Carvalho, P. M., Stolt, R. H., Matson, K. H., Coates, R. T., Corrigan, D., Foster, D. J., Shaw, S. A., and Zhang, H. 2003. Inverse scattering series and seismic exploration. *Inverse Problems* 19, R27–R83.

Weglein, A. B., Foster, D. J., Matson, K. H., Shaw, S. A., Carvalho, P. M., and Corrigan, D. 2001. An inverse-scattering sub-series for predicting the spatial location of reflectors without the precise reference medium and wave velocity. In *71st Annual Internat. Mtg., Soc. Expl. Geophys., Expanded Abstracts*. Soc. Expl. Geophys., 2108–2111.

Weglein, A. B., Gasparotto, F. A., Carvalho, P. M., and Stolt, R. H. 1997. An inverse-scattering series method for attenuating multiples in seismic reflection data. *Geophysics 62,* 6 (November-December), 1975–1989.

Weglein, A. B., Matson, K. H., Foster, D. J., Carvalho, P. M., Corrigan, D., and Shaw, S. A. 2000. Imaging and inversion at depth without a velocity model: Theory, concepts and initial evaluation. In *70th Annual Internat. Mtg., Soc. Expl. Geophys., Expanded Abstracts*. Soc. Expl. Geophys., 1016–1019.

Weglein, A. B. and Secrest, B. G. 1990. Wavelet estimation for a multidimensional acoustic earth model. *Geophysics 55,* 7 (July), 902–913.

Weglein, A. B., Shaw, S. A., Matson, K. H., Sheiman, J. L., Solt, R. H., Tan, T. H., Osen, A., Correa, G. P., Innanen, K. A., Guo, Z., and Zhang, J. 2002. New approaches to deghosting towed-streamer and ocean-bottem pressure measurements. In *72nd Annual Internat. Mtg., Soc. Expl. Geophys., Expanded Abstracts*. Soc. Expl. Geophys., 1016–1019.

Weglein, A. B., Tan, T. H., Matson, K. H., Shaw, S. A., and Foster, D. J. 2000. Prediction of the wavefield anywhere above an ordinary towed streamer: Applications to

source wavelet estimation, demultiple, and imaging. In *70th Annual Internat. Mtg., Soc. Expl. Geophys., Expanded Abstracts*. Soc. Expl. Geophys., 2413–2415.

Zhang, H. and Weglein, A. B. 2005a. The inverse scattering series for tasks associated with primaries: depth imaging and direct non-linear inversion of 1d variable velocity and density acoustic media. In *75th Annual Internat. Mtg., Soc. Expl. Geophys., Expanded Abstracts*. Soc. Expl. Geophys., 1705–1708.

Zhang, H. and Weglein, A. B. 2006. The inverse scattering series for tasks associated with primaries: direct non-linear inversion of 1d elastic media. In *76th Annual Internat. Mtg., Soc. Expl. Geophys., Expanded Abstracts*. Soc. Expl. Geophys., 2062–2066.

Zhang, J. and Weglein, A. B. 2005b. Extinction theorem deghosting method using towed streamer pressure data: Analysis of the receiver array effect on deghosting and subsequent free surface multiple removal. In *75th Annual Internat. Mtg., Soc. Expl. Geophys., Expanded Abstracts*. Soc. Expl. Geophys., 2095–2100.

APPENDICES

A. SOME NOTES ABOUT GREEN'S THEOREM

In this appendix, I discuss some interesting points that I learned from Prof. Weglein's Seismic Physics course. Among the points I discuss are: what is the function of the surface integration term in Green's Theorem and what is Extinction Theorem.

We start from the Green's Theorem (Green's Second Identity):

$$\begin{aligned}\int_V \Big(\psi(\mathbf{r}',\mathbf{r}_s,\omega)\nabla'^2\phi(\mathbf{r}',\mathbf{r},\omega) - \phi(\mathbf{r}',\mathbf{r},\omega)\nabla'^2\psi(\mathbf{r}',\mathbf{r}_s,\omega)\Big)\, d\mathbf{r}' \\ = \oint_S \left[\psi(\mathbf{r}',\mathbf{r}_s,\omega)\nabla'\phi(\mathbf{r}',\mathbf{r},\omega) - \phi(\mathbf{r}',\mathbf{r},\omega)\nabla'\psi(\mathbf{r}',\mathbf{r}_s,\omega)\right]\cdot d\mathbf{S}', \qquad \text{(A.1)}\end{aligned}$$

where $\psi(\mathbf{r}',\mathbf{r}_s,\omega)$ and $\phi(\mathbf{r}',\mathbf{r},\omega)$ are two arbitrary functions such that their second derivative and the integrations in Eq. A.1 exist. The closed surface S encloses volume V. We associate $\psi(\mathbf{r}',\mathbf{r}_s,\omega)$ with the pressure wavefield in the actual medium $P(\mathbf{r}',\mathbf{r}_s,\omega)$ which is assumed to satisfy

$$\nabla'^2 P(\mathbf{r}',\mathbf{r}_s,\omega) + \frac{\omega^2}{c^2(\mathbf{r}')}P(\mathbf{r}',\mathbf{r}_s,\omega) = A(\omega)\delta(\mathbf{r}'-\mathbf{r}_s) \qquad \text{(A.2)}$$

in the volume V and $A(\omega)$ is the source wavelet. Substituting $\frac{\omega^2}{c^2(\mathbf{r}')}$ with $k_0^2(1-\alpha(\mathbf{r}'))$ where $k_0^2 = \frac{\omega^2}{c_0^2}$, Eq. A.2 becomes

$$\nabla'^2 P(\mathbf{r}',\mathbf{r}_s,\omega) + k_0^2 P(\mathbf{r}',\mathbf{r}_s,\omega) \;=\; A(\omega)\delta(\mathbf{r}'-\mathbf{r}_s) + k_0^2\alpha(\mathbf{r}')P(\mathbf{r}',\mathbf{r}_s,\omega) \qquad \text{(A.3)}$$

where $\alpha(\mathbf{r}')$ represents the difference between the actual and reference medium.

We replace $\phi(\mathbf{r}', \mathbf{r}, \omega)$ with Green's function in the reference medium that satisfies:

$$\nabla'^2 G_0(\mathbf{r}', \mathbf{r}, \omega) + \frac{\omega^2}{c_0^2} G_0(\mathbf{r}', \mathbf{r}, \omega) = \delta(\mathbf{r}' - \mathbf{r}). \tag{A.4}$$

Substitute Eq. A.3 and Eq. A.4 into Eq. A.1, the LHS of Eq. A.1 becomes:

$$\begin{aligned} LHS &= \int_V P(\mathbf{r}', \mathbf{r}_s, \omega) \left(\delta(\mathbf{r}' - \mathbf{r}) - \frac{\omega^2}{c_0^2} G_0(\mathbf{r}', \mathbf{r}, \omega) \right) d\mathbf{r}' \\ &- \int_V G_0(\mathbf{r}', \mathbf{r}, \omega) \left(A(\omega)\delta(\mathbf{r}' - \mathbf{r}_s) + k_0^2 \alpha(\mathbf{r}') P(\mathbf{r}', \mathbf{r}_s, \omega) - \frac{\omega^2}{c_0^2} P(\mathbf{r}', \mathbf{r}_s, \omega) \right) d\mathbf{r}' \\ &= \int_V P(\mathbf{r}', \mathbf{r}_s, \omega)\delta(\mathbf{r}' - \mathbf{r}) d\mathbf{r}' \\ &- \int_V G_0(\mathbf{r}', \mathbf{r}, \omega) \left(A(\omega)\delta(\mathbf{r}' - \mathbf{r}_s) + k_0^2 \alpha(\mathbf{r}') P(\mathbf{r}', \mathbf{r}_s, \omega) \right) d\mathbf{r}' \end{aligned}$$

Combine LHS and RHS of Eq. A.1, we obtain

$$\begin{aligned} \int_V P(\mathbf{r}', \mathbf{r}_s, \omega)\delta(\mathbf{r}' - \mathbf{r}) d\mathbf{r}' &= \int_V G_0(\mathbf{r}', \mathbf{r}, \omega) \left(A(\omega)\delta(\mathbf{r}' - \mathbf{r}_s) + k_0^2 \alpha(\mathbf{r}') P(\mathbf{r}', \mathbf{r}_s, \omega) \right) d\mathbf{r}' \\ &+ \oint_S [P(\mathbf{r}', \mathbf{r}_s, \omega)\nabla' G_0(\mathbf{r}', \mathbf{r}, \omega) - G_0(\mathbf{r}', \mathbf{r}, \omega)\nabla' P(\mathbf{r}', \mathbf{r}_s, \omega)] \cdot d\mathbf{S}'. \end{aligned} \tag{A.5}$$

Eq. A.5 is correct for any volume V, any position $\mathbf{r}$, and any Green's function that satisfies Eq. A.4.

Assume $\mathbf{r}$ is inside of V, then

$$\begin{aligned} P(\mathbf{r}, \mathbf{r}_s, \omega) &= \int_V G_0(\mathbf{r}', \mathbf{r}, \omega) \left(A(\omega)\delta(\mathbf{r}' - \mathbf{r}_s) + k_0^2 \alpha(\mathbf{r}') P(\mathbf{r}', \mathbf{r}_s, \omega) \right) d\mathbf{r}' \\ &+ \oint_S [P(\mathbf{r}', \mathbf{r}_s, \omega)\nabla' G_0(\mathbf{r}', \mathbf{r}, \omega) - G_0(\mathbf{r}', \mathbf{r}, \omega)\nabla' P(\mathbf{r}', \mathbf{r}_s, \omega)] \cdot d\mathbf{S}'. \end{aligned} \tag{A.6}$$

Several points about Eq. A.6:

1. As long as P and $\nabla' P$ is causal on the surface S, then for any point inside V, a causal $P(\mathbf{r}, \mathbf{r}_s, \omega)$ will always be obtained, for *any* Green's function that satisfies Eq. A.4, *regardless of its causality and boundary conditions*. Chapter 2 demonstrates that different algorithms can be derived by using Green's function with different boundary conditions.

2. To predict the field at $\mathbf{r}$ inside of V, Eq. A.6 requires: medium information inside of V, and P and ∇P on the surface of V. Notice that these requirements are sufficient conditions to predict the field inside of V, they may not be necessary. In the field prediction algorithm in Chapter 2, for example, the derivative of P is not used since a special boundary condition of Green's function is used.

   The above mentioned "medium information inside of V" includes the medium properties and sources inside of V.

3. According to Lippmann-Schwinger equation, in order to know the field anywhere, we need to know the sources everywhere in the whole space:

$$P(\mathbf{r}, \mathbf{r}_s, \omega) = \int_{\infty} \rho(\mathbf{r}', \mathbf{r}_s) G_0^+(\mathbf{r}', \mathbf{r}, \omega) d\mathbf{r}' \tag{A.7}$$

$$= \int_{V} \rho(\mathbf{r}', \mathbf{r}_s) G_0^+(\mathbf{r}', \mathbf{r}, \omega) d\mathbf{r}' + \int_{U-V} \rho(\mathbf{r}', \mathbf{r}_s) G_0^+(\mathbf{r}', \mathbf{r}, \omega) d\mathbf{r}', \tag{A.8}$$

   where at the last step, the whole universe (U) is separated into two parts: V and $U - V$. Notice that in the Lippmann-Schwinger equation, we have to use G_0^+ in order to obtain the causal wavefield. The first term in Eq. A.8 represents part of the wavefield due to sources inside of V and the second term represents the part of the wavefield due to sources outside of V.

   To compare Eq. A.6 with Eq. A.8, we denote $A(\omega)\delta(\mathbf{r}' - \mathbf{r}_s) + k_0^2 \alpha(\mathbf{r}') P(\mathbf{r}', \mathbf{r}_s, \omega)$

as $\rho(\mathbf{r}', \mathbf{r}_s)$, and *choose* Green's function as causal Green's function, then Eq. A.6 becomes:

$$\begin{aligned} P(\mathbf{r}, \mathbf{r}_s, \omega) &= \int_V \rho(\mathbf{r}', \mathbf{r}_s) G_0^+(\mathbf{r}', \mathbf{r}, \omega) d\mathbf{r}' \\ &+ \oint_S \left[P(\mathbf{r}', \mathbf{r}_s, \omega) \nabla' G_0^+(\mathbf{r}', \mathbf{r}, \omega) - G_0^+(\mathbf{r}', \mathbf{r}, \omega) \nabla' P(\mathbf{r}', \mathbf{r}_s, \omega) \right] \cdot d\mathbf{S}'. \end{aligned} \tag{A.9}$$

Comparing Eq. A.9 and Eq. A.8, we conclude that the surface integration in Eq. A.9 generates part of the wavefield at $\mathbf{r}$ (inside of V) due to sources outside of V, since it equals the second integration term in Eq. A.8.

Note: This conclusion is obtained under the condition that causal Green's function, causal P and ∇P are used in the surface integration term.

Another way of understanding this conclusion using Extinction Theorem is: when $\mathbf{r}$ is *inside* of V, although P and ∇P are contributed by sources both inside and outside of V, if we use a causal Green's function, then the surface integration will *extinguish* the contributions due to sources *inside* of V, only contributions from sources *outside* of V will be kept.

Assume $\mathbf{r}$ is outside of V, and choose causal Green's function, then Eq. A.5 becomes

$$\begin{aligned} 0 &= \int_V \rho(\mathbf{r}', \mathbf{r}_s) G_0^+(\mathbf{r}', \mathbf{r}, \omega) d\mathbf{r}' \\ &+ \oint_S \left[P(\mathbf{r}', \mathbf{r}_s, \omega) \nabla' G_0^+(\mathbf{r}', \mathbf{r}, \omega) - G_0^+(\mathbf{r}', \mathbf{r}, \omega) \nabla' P(\mathbf{r}', \mathbf{r}_s, \omega) \right] \cdot d\mathbf{S}', \end{aligned} \tag{A.10}$$

where we again denote $A(\omega)\delta(\mathbf{r}' - \mathbf{r}_s) + k_0^2 \alpha(\mathbf{r}') P(\mathbf{r}', \mathbf{r}_s, \omega)$ as $\rho(\mathbf{r}', \mathbf{r}_s)$. Since Eq. A.8 is valid

everywhere, we subtract Eq. A.8 by Eq. A.10 to obtain:

$$\begin{aligned} P(\mathbf{r}, \mathbf{r}_s, \omega) &= \int_{U-V} \rho(\mathbf{r}', \mathbf{r}_s) G_0^+(\mathbf{r}', \mathbf{r}, \omega) d\mathbf{r}' \\ &- \oint_S \left[P(\mathbf{r}', \mathbf{r}_s, \omega) \nabla' G_0^+(\mathbf{r}', \mathbf{r}, \omega) - G_0^+(\mathbf{r}', \mathbf{r}, \omega) \nabla' P(\mathbf{r}', \mathbf{r}_s, \omega) \right] \cdot d\mathbf{S}' \end{aligned} \quad \text{(A.11)}$$

Since we already know the volume integration term in Eq. A.11 generates part of the causal field due to source outside of V, so the surface integration term in Eq. A.11 generates the causal field due to source inside of V. This is the other interesting point of the Extinction Theorem: although P and ∇P are due to sources both inside and outside of V, if we use a causal Green's function and point $\mathbf{r}$ is outside of V, then the surface integration will *extinguish* contributions due to source *outside* of V, only contributions from source *inside* of V will be kept.

Combining the two points of the Extinction Theorem, we conclude that: (1) Extinction Theorem is just a special case of Green's Theorem since only causal Green's function can be used; (2) the surface integration in Green's/Extinction Theorem will extinguish contributions from sources inside of V, if $\mathbf{r}$ is inside of V, and (3) the surface integration will extinguish contributions from sources outside of V, if $\mathbf{r}$ is outside of V.

B. DERIVATION OF $2D$ G_0^{DD}

We assume that the source is at (ξ, η), and the free surface and the measurement surface are at $y = 0$ and $y = b$ respectively. We will try to find the solution of the following partial differential equations:

$$\nabla^2 G + k^2 G = \delta(x|\xi; y|\eta), \tag{B.1}$$

with the Dirichlet conditions on $y = 0$ and $y = b$.

Assuming

$$G_0^{DD}(x|\xi; y|\eta) = \sqrt{\frac{2}{b}} \sum_{n=1}^{\infty} g_n(x) \sin(\frac{n\pi}{b} y), \tag{B.2}$$

and substituting Eq. B.2 into Eq. B.1, and using $\sqrt{\frac{2}{b}} \sin(\frac{m\pi}{b} y)$ multiply both sides of Eq. B.1, integrating over y from 0 to b, we obtain

$$\frac{d^2}{dx^2} g_m(x) - (\frac{m^2\pi^2}{b^2} - k^2) g_m(x) = \sqrt{\frac{2}{b}} \sin(\frac{m\pi}{b}\eta)\delta(x - \xi). \tag{B.3}$$

Assume $k_x^2 = \frac{m^2\pi^2}{b^2} - k^2 > 0$ (i.e. for $b = 6.0m, c = 1500m/s, f$ should be less than $125Hz$),

for physical solution ($g_,(x) < \infty$, as $x \to \infty$), we choose

$$\begin{cases} g_m(x) = Ae^{k_x x}, & \text{for } x < \xi \\ g_m(x) = Be^{-k_x x}, & \text{for } x > \xi. \end{cases}$$

On $x = \xi$, we have

$$\begin{cases} Ae^{k_x \xi} & = Be^{-k_x \xi} \\ -k_x Be^{-k_x \xi} - Ak_x e^{k_x \xi} & = \sqrt{\frac{2}{b}} \sin(\frac{m\pi}{b}\eta), \end{cases}$$

i.e.

$$\begin{cases} A & = -\frac{1}{k_x}\sqrt{\frac{1}{2b}} \sin(\frac{m\pi}{b}\eta) e^{-k_x \xi} \\ B & = -\frac{1}{k_x}\sqrt{\frac{1}{2b}} \sin(\frac{m\pi}{b}\eta) e^{k_x \xi} \end{cases}$$

So

$$g_m(x) = -\frac{1}{k_x}\sqrt{\frac{1}{2b}} \sin(\frac{m\pi}{b}\eta) e^{-k_x |x-\xi|}.$$

Finally

$$\begin{aligned} G_0^{DD}(x|\xi; y|\eta) &= \sqrt{\frac{2}{b}} \sum_{n=1}^{\infty} g_n(x) \sin(\frac{n\pi}{b} y) \\ &= -\frac{1}{b} \sum_{n=1}^{\infty} \frac{1}{\sqrt{\frac{n^2\pi^2}{b^2} - k^2}} \sin(\frac{n\pi}{b}\eta) e^{-\sqrt{\frac{n^2\pi^2}{b^2} - k^2}|x-\xi|} \sin(\frac{n\pi}{b} y) \end{aligned} \tag{B.4}$$

and

$$\frac{\partial G_0^{DD}(x|\xi;y|\eta)}{\partial y} = -\frac{\pi}{b^2}\sum_{n=1}^{\infty} n\frac{1}{\sqrt{\frac{n^2\pi^2}{b^2}-k^2}}\sin(\frac{n\pi}{b}\eta)e^{-\sqrt{\frac{n^2\pi^2}{b^2}-k^2}|x-\xi|}\cos(\frac{n\pi}{b}y) \quad \text{(B.5)}$$

Obviously, the G_0^{DD} above vanishes both on $y = 0$ and $y = b$. And both G_0^{DD} and its derivative vanishes exponentially when $|x - \xi|$ increases.

Other approaches and discussions of G_0^{DD} can be found in Tan (1999) and Osen *et al.* (1998).